THE PLANT CELL

Research Article

The phospholipid flippase ALA3 regulates pollen tube growth and guidance in Arabidopsis

Yang Yang (iD) ,[1] Yue Niu (iD) ,[1] Tao Chen (iD) ,[1] Hongkai Zhang (iD) ,[1] Jingxia Zhang (iD) ,[1] Dong Qian (iD) ,[1] Mengmeng Bi,[1] Yuemin Fan (iD) ,[1] Lizhe An (iD) [1] and Yun Xiang (iD) [1,*]

1 MOE Key Laboratory of Cell Activities and Stress Adaptations, School of Life Sciences, Lanzhou University, Lanzhou 730000, China

*Author for correspondence: xiangy@lzu.edu.cn
These authors contributed equally (Y.Y. and Y.N.).
Y.X., Y.Y., and Y.N. conceived the study and designed the research; Y.Y., T.C., J.Z., and H.Z. performed the research; Y.Y., Y.N., T.C., J.Z., H.Z., D.Q., M.B., Y.F., and L.A. analyzed the data; Y.X., Y.Y., Y.N., H.Z., and D.Q. wrote the manuscript.
The author responsible for the distribution of materials integral to the findings presented in this article in accordance with the policy described in the Instructions for Authors (https://academic.oup.com/plcell) is: Yun Xiang (xiangy@lzu.edu.cn).

Abstract

Pollen tube guidance regulates the growth direction and ovule targeting of pollen tubes in pistils, which is crucial for the completion of sexual reproduction in flowering plants. The Arabidopsis (*Arabidopsis thaliana*) pollen-specific receptor kinase (PRK) family members PRK3 and PRK6 are specifically tip-localized and essential for pollen tube growth and guidance. However, the mechanisms controlling the polar localization of PRKs at the pollen tube tip are unclear. The Arabidopsis P4-ATPase ALA3 helps establish the polar localization of apical phosphatidylserine (PS) in pollen tubes. Here, we discovered that loss of ALA3 function caused pollen tube defects in growth and ovule targeting and significantly affected the polar localization pattern of PRK3 and PRK6. Both PRK3 and PRK6 contain two polybasic clusters in the intracellular juxtamembrane domain, and they bound to PS in vitro. PRK3 and PRK6 with polybasic cluster mutations showed reduced or abolished binding to PS and altered polar localization patterns, and they failed to effectively complement the pollen tube-related phenotypes of *prk* mutants. These results suggest that ALA3 influences the precise localization of PRK3, PRK6, and other PRKs by regulating the distribution of PS, which plays a key role in regulating pollen tube growth and guidance.

Introduction

Flowering plants have a unique, complex reproduction process known as double fertilization, which involves pollen grain hydration and germination on the stigma, the delivery of two sperm cells to the embryo sac through the growing pollen tube, and the subsequent fusion of the sperm cells with the egg and central cell to generate the embryo and endosperm, respectively. During the long journey of the pollen tube, vast male–female communication networks are needed for successful double fertilization (McCormick, 2004; Berger et al., 2008; Zhong and Qu, 2019). Pollen tube guidance is a major stage in the persistent interaction between

male and female gametophytes. This process is divided into two phases: preovular guidance and ovular guidance (Lausser and Dresselhaus, 2010; Higashiyama and Takeuchi, 2015). Preovular guidance involves pollen grain germination on the stigma and pollen tube growth along the transmitting tract through the septum. Ovular guidance involves two phases: (1) funicular guidance, in which the growth direction of the pollen tube is altered toward the funiculus and the pollen tube continues to grow along the funiculus and (2) micropylar guidance, in which the pollen tube reaches near the micropyle, turns toward a micropyle

Open Access

IN A NUTSHELL

Background: In flowering plants, pollen tube guidance regulates the rapid growth and timely targeting of the pollen tube to the ovule in the pistil during sexual reproduction, when signaling between the male and female gametophytes occur. The small peptide-RLK signaling module is essential for the interaction between the male and female gametophyte. Certain members of the pollen-specific receptor kinase (PRK) family have different sub-cellular localization patterns in Arabidopsis pollen tubes and play critical roles in pollen tube growth and guidance. However, the molecular mechanisms that regulate and maintain the polar localization of PRKs at the pollen tube tip are still unknown.

Question: We were interested in exploring how Arabidopsis P4-ATPase (aminophospholipid ATPase, ALA) precisely regulates pollen tube guidance and maintains the polar localization patterns of PRK6 and PRK3. How plant ALA family members regulate pollen tube guidance has not yet been documented.

Findings: The loss of ALA3 function not only caused sluggish pollen tube growth and aberrant ovule targeting but also affected the polar localization patterns of several PRKs at the pollen tube tip. Members of the PRKs family can directly interact with anionic phospholipids such as phosphatidylserine (PS), and the capacity of PRK3/6 to bind anionic phospholipids is crucial for both their polar localization and physiological functions. ALA3 establishes and maintains the polar distribution of PS, which influences secretory vesicles-mediated polar trafficking at the pollen tube tip to affect the distribution of PRK3 and PRK6. On the other hand, PS might also directly recruit PRK3 and PRK6 to the pollen tube tip and sustain their localization.

Next steps: The localization of PRKs is a complex, finely regulated process. The C-termini of PRKs may also affect their polar distribution. More research is required to reveal how the C-terminus domain precisely controls the localization of PRKs.

opening, and ultimately enters the embryo sac via a filiform apparatus to interact with receptive synergid cells (Shimizu and Okada, 2000; Higashiyama and Takeuchi, 2015).

Various small peptides secreted by the stigma and by male and female gametophytes are important signaling molecules that regulate diverse reproductive processes, including pollen grain hydration and germination and pollen tube growth, guidance, and rupture (Muschietti et al., 1994; Liu et al., 2021; Takeuchi, 2021; Yu et al., 2021). Small peptides are perceived by different receptor-like kinases (RLKs) of pollen tubes to activate relevant signaling pathways. Therefore, the peptide-RLK signaling complex of angiosperms plays a key role in male–female interactions (Johnson et al., 2019; Zhang et al., 2021). After germination on the stigma, rapid pollen tube growth and effective targeting to ovules during pollen tube guidance depend on the response to small peptides secreted by the stigma, transmitting tract and female gametophyte.

Some small peptides secreted by the stigma and transmitting tract regulate pollen grain germination on the stigma and the rapid growth of pollen tubes in the transmitting tract; some examples include the glycosylated polypeptides LAT52 (Muschietti et al., 1994; Tang et al., 2002) and STIGMA-SPECIFIC PROTEIN1 (LeSTG1; Tang et al., 2004; Huang et al., 2014) in tomato (*Solanum lycopersicum*) and CLE45 in Arabidopsis (Endo et al., 2013). Some small peptides that are exclusively expressed in the egg apparatus (egg cell and synergid cell) are vital signaling molecules needed for pollen tube guidance to the micropylar. Examples of these peptides include Egg Apparatus 1 (ZmEA1) in maize

(*Zea mays*; Márton et al., 2005); TfLURE1 and TfLURE2, which are cysteine-rich polypeptides in the defensin-like protein family in *Torenia fournieri* (Okuda et al., 2009); AtLURE1 peptides, which are functional homologs of TfLUREs in *A. thaliana* (Takeuchi and Higashiyama, 2012; Zhong et al., 2019); and the cysteine-rich peptide XIUQIUs and TICKETs in *A. thaliana* (Meng et al., 2019; Zhong and Qu, 2019; Liu et al., 2021). ZmEA1, AtLURE1, and AtTICKET2 are involved in micropylar guidance and act as female attractants with species-specific preferences (Márton et al., 2005; Takeuchi and Higashiyama, 2012; Meng et al., 2019; Zhong and Qu, 2019).

Pollen-specific receptor kinases (PRKs) are RLKs that contain six leucine-rich repeat (LRR) domains and are expressed abundantly in pollen. Several PRKs sense the small peptides mentioned above and play key roles in pollen germination, pollen tube growth, pollen tube guidance, interspecific reproductive isolation, and fertility (Zhang et al., 2008; Zhao et al., 2013; Duckney et al., 2017; Guo and Yang, 2020). LePRK2 combined with pollen-specifically expressed LAT52 regulates pollen germination and early pollen tube growth in tomato (Tang et al., 2002). The small peptide LeSTG1 expressed by the stigma competitively replaces LAT52 to bind LePRK2 in growing pollen tubes and participates in the regulation of pollen tube growth in tomato (Tang et al., 2004; Huang et al., 2014).

Many PRK family members participate in pollen tube growth in Arabidopsis in vivo. For example, the multiple mutants *prk3 prk6*, *prk1 prk3 prk6*, and *prk3 prk6 prk8* show slow-growing pollen tubes in the transmitting tract

and seed abortion phenotypes. PRK6 is an essential receptor in the sensing of the attractant peptide LURE1.2: the *prk6* mutant fails to target nearby ovules in vivo and shows no response to LURE1.2, as observed in a semi-in-vivo assay (Takeuchi and Higashiyama, 2016). Moreover, LOST IN POLLEN TUBE GUIDANCE 1 (LIP1) and LIP2 belong to the receptor-like cytoplasmic kinase VII subfamily, and MALE DISCOVERER 1 (MDIS1) and MDIS2 combine with MDIS1-INTERACTING RECEPTOR LIKE KINASE 1 (MIK1) and MIK2 to form a receptor complex, which is also involved in the recognition of LURE1 signaling (Liu et al., 2013; Wang et al., 2016). A structural study demonstrated that the extracellular domain of PRK6 is bound by LURE1.2 (Zhang et al., 2017). PRK6 also interacts with its homologous protein PRK3, RopGEFs and LIP1/2 (Takeuchi and Higashiyama, 2016; Yu et al., 2018). These findings indicate that the PRK6 receptor is responsible for sensing extracellular LURE1 and triggering cytoplasmic LIP1/2 and RopGEFs to achieve downstream signal transduction (Liu et al., 2013; Takeuchi and Higashiyama, 2016; Zhang et al., 2017). The LURE1–PRK6 signaling pathway also specifically promotes rapid conspecific pollen tube growth and micropylar attraction activity, which are indispensable for reproductive isolation in *A. thaliana* (Zhong and Qu, 2019; Liu et al., 2021). However, gaps in the knowledge of the mechanisms regulating pollen tube guidance and other ligands of other PRKs remain.

In pollen tubes, the subcellular location and distribution of PRK family members differ. PRK6 specifically localizes to the apical plasma membrane and inverted cone zone of the pollen tube, regardless of whether the pollen germination medium contains LURE1.2. Exogenous treatment with LURE1.2 induced the remodeling of the apical localization pattern of PRK6. Specifically, treatment with this attractant caused PRK6 to asymmetrically accumulate toward the direction of exogenous LURE1.2, ultimately altering the growth direction of the pollen tube toward LURE1.2 (Takeuchi and Higashiyama, 2016). The remodeled tip localization of PRK6 induced by LURE1.2 plays a key role in controlling the direction of pollen tube tip growth.

Another member of the PRK family, PRK3, shows a polar localization pattern at the tip similar to that of PRK6 (Takeuchi and Higashiyama, 2016). The other three members of the PRK family in *A. thaliana*, PRK2, PRK4, and PRK5, are mainly distributed in the shank plasma membrane of the pollen tube (Zhao et al., 2013; Wrzaczek et al., 2015; Duckney et al., 2017). Analysis of PRK2 lacking specific functional domains showed that deleting the juxtamembrane (JM) domain significantly reduced the localization of PRK2 on the shank plasma membrane and that PRK2 lacking the JM and carboxy-terminal domains could not localize to the plasma membrane. The kinase activity of PRK2 does not affect its plasma membrane localization. These findings suggest that the JM and carboxy-terminal domains are essential for the localization of PRK2 (Zhao et al., 2013). However, the precise mechanism underlying the maintenance of the polar localization of PRK3 and PRK6 at the pollen tube tip and

the molecular mechanism controlling the different subcellular localizations of PRK family members are unclear.

Type IV P-type ATPases (P4-ATPases) are a class of eukaryotic-specific phospholipid flippases that flip aminophospholipids such as phosphatidylcholine, phosphatidylethanolamine, and phosphatidylserine (PS) from the extracellular/luminal leaflet of the plasma membrane/organelles to the cytoplasmic side. This process, which is powered by ATP hydrolysis, establishes and maintains the asymmetric distribution of phospholipids within the plasma membrane (Roland and Graham, 2014; López-Marqués, 2021). In addition, P4-ATPases are involved in endosomal trafficking (Pomorski et al., 2003; Poulsen et al., 2008; Muthusamy et al., 2009). Most P4-ATPases are heterodimers consisting of a catalytic α subunit with 10 transmembrane domains and an auxiliary β-subunit with two transmembrane domains (Palmgren and Nissen, 2011; Andersen et al., 2016).

The catalytic subunit family of Arabidopsis P4-ATPases comprises 12 members, also termed Aminophospholipid ATPases 1–12 (ALA1–ALA12). Arabidopsis ALAs play key roles in many processes, including plant growth and development, reproduction, and responses and resistance to biotic and abiotic stress (Gomès et al., 2000; McDowell et al., 2013, 2015, 2018; Poulsen et al., 2015; Guo et al., 2017; Niu et al., 2017; Zhang et al., 2020; López-Marqués, 2021; Wang et al., 2021). Six members of the Arabidopsis ALA family are abundantly expressed in pollen. To date, only ALA3, ALA6, and ALA7 have been proven to be involved in pollen development and pollen tube growth. For example, the pollen tube of *ala6 ala7* double mutants grows slowly, and the plasma membrane cannot be effectively stained by the lipophilic dye FM4–64 (McDowell et al., 2015). ALA3 is also involved in trichome development and pollen tube growth, and the loss of its function causes a decrease in the pollen tube growth rate and a cyclosis (cytoplasmic streaming) disorder in the pollen tube shank (Zhang and Oppenheimer, 2009; McDowell et al., 2013, 2018). ALA3 deficiency also leads to an apparent increase in pollen tube width; moreover, ALA3 is involved in establishing and maintaining the polar distribution of PS at the pollen tube tip and in controlling Rab GTPase-mediated vesicle trafficking (Zhou et al., 2020). However, whether and/or how ALAs coordinate pollen tube guidance is unclear.

In the present study, we found that the loss of ALA3 function resulted in defects in pollen tube growth and guidance and disturbances in the polar localization of PRK3 and PRK6 at the pollen tube tip. We also uncovered the potential mechanism underlying the binding of PRK family members to anionic phospholipids and revealed the differences in the subcellular localizations of these proteins. Our findings indicate that ALA3 plays an important role in the guidance and rapid growth of pollen tubes by maintaining the polar distribution of the specific anionic phospholipid PS in the tips of pollen tubes to regulate the precise tip localization of PRK3 and PRK6.
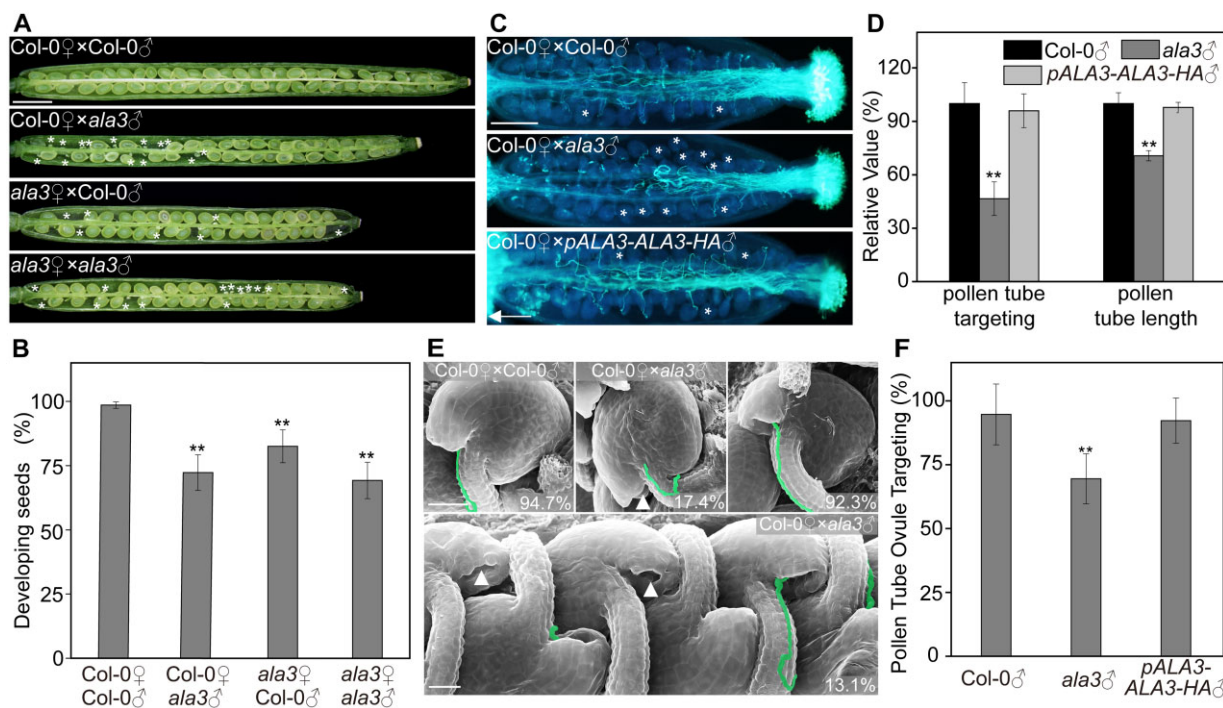
Figure 1 The *ala3* mutants show defects in pollen tube growth, guidance and fertility. A, Developing seeds in siliques 10 days after reciprocal crosses between Columbia-0 (Col-0) plants and *ala3* mutants. The images are representative of 15 samples. Asterisks indicate unfertilized ovules, which were counted as aborted seeds. Scale bar: 1 mm. B, Statistical analysis of developing seeds in (A). Three independent examinations were performed. The data are presented as the mean ± SDS ($n = 15$). **$P < 0.01$ (t test compared with wild-type values). C, Pollen tubes of Col-0, *ala3*, and *pALA3-ALA3-HA* growing in Col-0 pistils. Aniline blue staining was performed 8 HAP. The asterisks mark ovules that did not attract near pollen tubes. The arrow points to the bottom of the pistil. The data are representative of 15 samples for each genotype. Scale bar: 100 μm. D, Statistical analysis of the ovule-targeting efficiency and length of pollen tubes in (C). Three independent examinations were performed. The data are presented as the mean ± SDS ($n = 15$). **$P < 0.01$ (t test compared with wild-type values). E, Scanning electron microscopic observations of pollen tube guidance in Col-0 and *ala3* plants 17 h after limited hand pollinations onto Col-0 pistils. The arrowheads indicate micropyles. Scale bar: 20 μm. The data are representative of at least three independent examinations. F, Statistical analysis of the ovule-targeting efficiency of pollen tubes in (E). Three independent examinations were performed. The data are presented as the mean ± SDS ($n \geqslant 290$). **$P < 0.01$ (t test, compared with wild-type values).

Table 1 Transmission efficiency test through reciprocal crossing.

Parent (♀ × ♂)	Cross description	Assay	Expected (%)	Observed (%)	n	P value
Col-0 × *ala3*(+ /−)	Male outcross	*ala3*(−)	50	25.4	382	< 0.001
ala3(+ /−) × Col-0	Female outcross	*ala3*(−)	50	51.8	362	0.116
ala3(+ /−) × same	Selfed	*ala3*(−/−)	25	14.2	384	< 0.001

Col-0 is the wild-type. The observed results were compared to the expected Mendelian segregation ratio. Statistical significance was determined by the Pearson's Chi-squared test.

Results

Loss of ALA3 function induces defects in pollen tube growth, guidance, and fertility

We recently discovered that ALA3 is involved in regulating pollen tube growth and maintaining pollen tube width (Zhou et al., 2020). Compared to wild-type plants, siliques in *ala3* mutant plants were shorter and wider, but this wider morphology was only observed in mature siliques (Supplemental Figure S1, A and B). The average number of developing seeds in each wild-type silique was approximately 50–60, whereas only 30–40 developing seeds were detected in *ala3* siliques. To determine which gametophyte defects are chiefly

responsible for seed abortion, we performed a reciprocal cross between wild-type and *ala3* plants. Regardless of whether the *ala3* mutant was the paternal or maternal parent, the resulting siliques had a lower number of developing seeds (Figure 1, A and B). This result suggests that the loss of ALA3 function causes defects in both male and female gametophytes. Subsequent analysis of the transmission rate indicated that the male transmission rate was 25.4% in *ala3* mutants, which was significantly lower than the expected rate of 50%, but the female transmission rate was normal (Table 1). Thus, our subsequent research focused on determining how the male gametophyte of the *ala3* mutants causes seed abortion.

Pollen tube guidance regulates the direction of pollen tube tip growth and timely ovule targeting. We examined whether pollen tube guidance was abnormal in the *ala3* mutant in vivo. At 9-h after pollination (HAP), wild-type pollen tubes reached the bottom of the pistil, whereas the *ala3* mutant pollen tube grew slowly and ultimately reached the bottom of the pistil at 17 HAP (Supplemental Figure S1C). We subsequently examined whether ovule targeting of the *ala3* pollen tube was affected. We pollinated *ala3* mutant pollen onto wild-type stigmas and detected the ovule targeting of the pollen tube by aniline blue staining. Most wild-type pollen tubes were attracted to nearby ovules on the septum surface, whereas the *ala3* mutant pollen tubes showed a wandering phenotype and failed to target nearby ovules (Figure 1, C and D). These behaviors of the *ala3* mutant indicate that the pollen tubes were insensitive to ovule attraction, although ∼70% of the pollen tubes were ultimately successfully attracted by the ovules.

Through an aniline blue staining assay, we verified the phenotypes of pollen tube growth and ovule targeting in the *pALA3–ALA3–HA* complementation lines and discovered that ALA3 rescued the phenotypes of slow pollen tube growth and aberrant ovule targeting in the *ala3* mutant (Supplemental Figure S1D; Figure 1, C and D). Scanning electron microscopy showed that 94.7% of wild-type pollen tubes (*n* = 324) entered the micropyle rapidly and accurately, and 30.5% of *ala3* mutant pollen tubes (*n* = 292) were off-target, which was considerably higher than the corresponding off-target percentage of wild-type pollen tubes (Figure 1, E and F). Nearly 17.4% of the *ala3* mutant pollen tubes grew along the funiculus and passed by the micropyle without entering. Approximately 13.1% of the *ala3* mutant pollen tubes were not found in the funiculus, and the micropyle and failed to enter the ovules because they did not climb up the funiculus or appear on the other side of the ovule. Expressing *pALA3–ALA3–HA* in the *ala3* mutant rescued the guidance defect of *ala3* pollen tubes (Figure 1F). These results indicate that the reduced male transmission observed in *ala3* mutants is mainly due to defective pollen tube guidance toward the micropyle, which suggests that ALA3 plays a critical role in guiding pollen tubes into the micropyle. Overall, these results suggest that loss of ALA3 function causes defects in pollen tube growth and ovule targeting in vivo, and these defects result in abortion.

The distribution pattern of PRKs is altered in *ala3* mutant pollen tubes

The PRK family has eight members in *A. thaliana*, and *prk6* mutant pollen tubes failed to rapidly target the ovules. The pollen tubes of the *prk3 prk6* double mutant grew slowly and exhibited abnormal guidance. A certain proportion of abortion was observed in the *prk3 prk6* double mutant, and the abortion phenotypes of the *prk1 prk3 prk6* and *prk3 prk6 prk8* triple mutants were more severe. However, *prk1 prk2 prk4 prk5* quadruple mutants show no pollen tube-related or abortion phenotypes (Takeuchi and Higashiyama, 2016).

Therefore, to verify the relationship between ALA3 and PRKs, we observed the localization of PRK1, PRK3, PRK6, and PRK8 in *ala3* mutant pollen tubes. PRK6–mRuby2 (Figure 2, A and C; Supplemental Movie S1 and PRK3–mClover [Figure 2, F and H; Supplemental Movie S2]) were located in the apical plasma membrane, the apical membrane-proximal region and the inverted-cone zone. PRK1–GFP was distributed in the apical plasma membrane, the shank plasma membrane and the inverted-cone zone (Figure 2, K and M). PRK8–GFP was mainly distributed in the shank plasma membrane but weakly distributed in the apical membrane and the apical inverted-cone zone (Figure 2, P and R).

Since the localization patterns of the abovementioned PRKs were altered to different degrees in *ala3* pollen tubes, we quantified fluorescence signals from PRK fusion proteins in five regions of the pollen tube: the apical membrane-proximal region (i), apical plasma membrane (ii), subapical cytoplasm (iii), subapical plasma membrane (iv), and shank plasma membrane (v) (Figure 2U). The fluorescence signals of PRK6–mRuby2 (Figure 2, B, D, and V; Supplemental Movie S3), PRK3–mClover (Figure 2, G, I, and W; Supplemental Movie S4), and PRK1–GFP (Figure 2, L, N and X) were markedly reduced in the apical membrane-proximal region and apical plasma membrane in *ala3* pollen tubes and aggregated on two sides of the subapical cytoplasm. The fluorescence signals of PRK6–mRuby2 increased in the subapical plasma membrane of *ala3 prk6* pollen tubes, but the localization of PRK3–mClover and PRK1–GFP in the subapical plasma membrane showed no significant difference. The distribution of PRK1–GFP in the shank plasma membrane did not present a clear difference. The fluorescence signals of PRK8–GFP were notably reduced in the apical membrane-proximal region and the shank plasma membrane in *ala3* pollen tubes (Figure 2, Q, S, and Y).

The three other members of the PRK family in *A. thaliana*, PRK2–GFP (Supplemental Figure S2, A and C), PRK4–GFP (Supplemental Figure S2, E and G), and PRK5–GFP (Supplemental Figure S2, I and K), were mainly distributed in the shank plasma membranes of wild-type pollen tubes. A slight distribution of PRK4 was observed in the apical membrane-proximal region, and the fluorescence signal of PRK4–GFP was reduced in the apical membrane-proximal region in *ala3* pollen tubes (Supplemental Figure S2, F and H). The distribution patterns of PRK2–GFP (Supplemental Figure S2, B and D) and PRK5–GFP (Supplemental Figure S2, J and L) were not altered in *ala3* mutant pollen tubes. In conclusion, the loss of ALA3 function results in significant changes in the polar distribution patterns of PRK6 and other PRKs related to pollen tube growth at the tip, which may be the main reasons for the slow pollen tube growth, abnormal guidance, and embryo abortion phenotypes of the *ala3* mutant.

RabA4d-mediated vesicle trafficking regulates the polar distribution of PRK6 at the pollen tube tip

We previously reported that ALA3 regulates the PS-mediated polar distribution pattern of the Rab GTPase
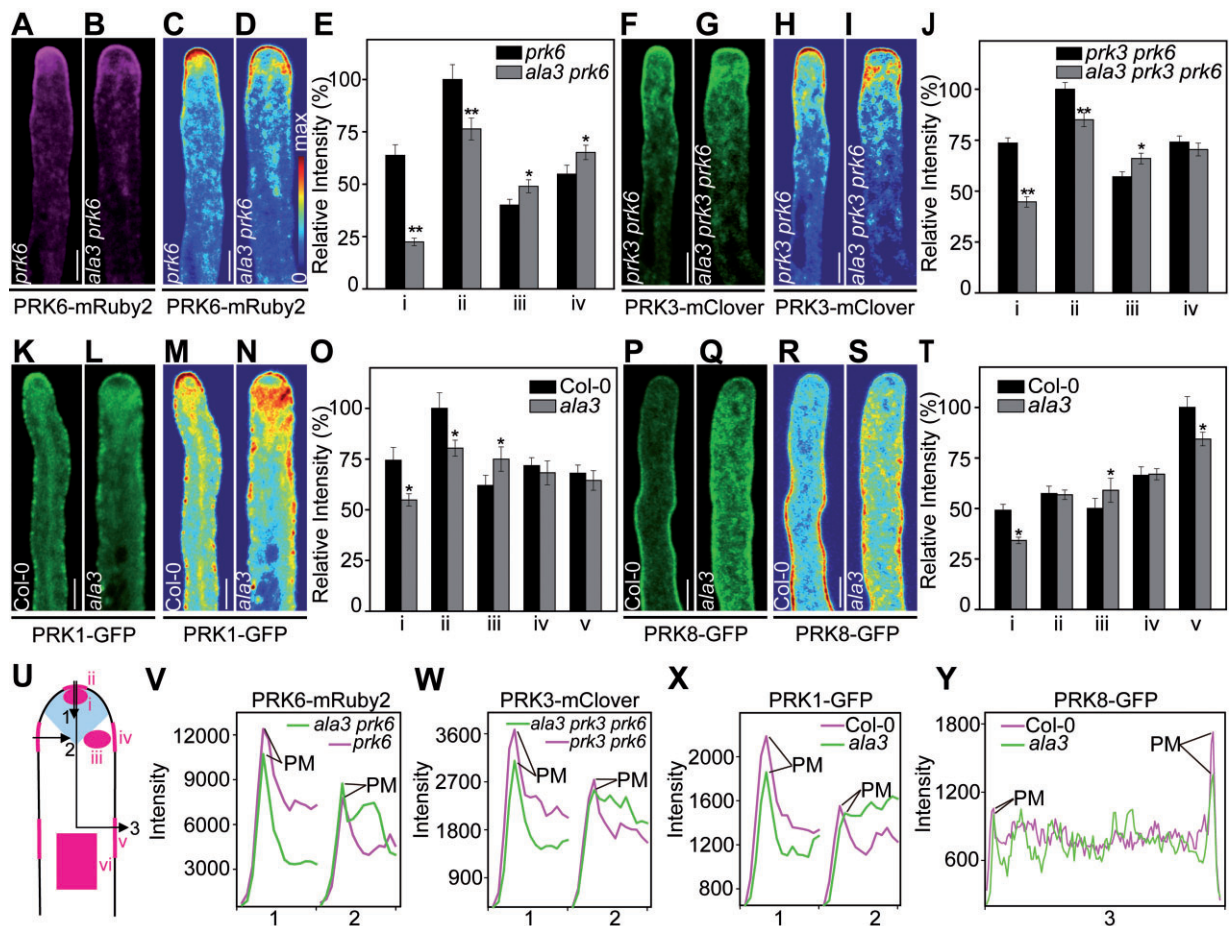
Figure 2 The loss of ALA3 function leads to an altered distribution pattern of PRKs. A–D, Representative confocal images of pollen tube localization of PRK6-mRuby2 in *prk6* (A) and *ala3 prk6* mutants (B) from the same transgenic line and pseudocolor images of its intensity (C) and (D). Scale bar: 5 μm. F–I, Representative confocal images of pollen tube localization of PRK3–mClover in *prk3 prk6* (F) and *ala3 prk3 prk6* mutants (G) from the same transgenic line and pseudocolor images of its intensity (H) and (I). Scale bar: 5 μm. K–N, Representative confocal images of pollen tube localization of PRK1–GFP in Col-0 plants (K) and *ala3* mutants (L) from the same transgenic line and pseudocolor image of its intensity (M) and (N). Scale bar: 5 μm. P–S, Representative confocal images of pollen tube localization of PRK8–GFP in Col-0 plants (P) and *ala3* mutants (Q) from the same transgenic line and pseudocolor image of its intensity (R) and (S). Scale bar: 5 μm. E, J, O, and T, Quantitative analysis of the relative fluorescence intensity of PRK6–mRuby2 (E), PRK3–mClover (J), PRK1–GFP (O), and PRK8–GFP (T) in the apical membrane-proximal region (i), apical plasma membrane (ii), subapical cytoplasm (iii), subapical plasma membrane (iv), and shank plasma membrane (v) shown in (U). The results are presented as the means ± SES ($n = 30$). *$P < 0.05$; **$P < 0.01$ (t test compared with the wild-type values). U, Schematic drawing of a pollen tube. The apical membrane-proximal region (i), apical plasma membrane (ii), subapical cytoplasm (iii), subapical plasma membrane (iv), shank plasma membrane (v), and shank cytoplasm (vi) are shown in magenta, and the inverted-cone zone is shown in blue. The (1), (2), and (3) positions marked with arrows were used for plot profile analysis. V–Y, Plot profile analysis of the changes in the fluorescence signals of PRK6-mRuby2 (V), PRK3–mClover (W), PRK1–GFP (X), and PRK8–GFP (Y) at the (1), (2), and (3) positions marked with arrows shown in (U).

RabA4d at the pollen tube tip by establishing and maintaining the polar distribution of PS. Growing *raba4d* mutant pollen tubes grew more slowly and had wider tips than the wild-type (Zhou et al., 2020). The absence of RabA4d function leads to reductions in the targeting efficiency of pollen tubes to ovules in vivo (Szumlanski and Nielsen, 2009). To determine whether the *ala3* mutant phenotype related to pollen tube guidance is caused by the effect of RabA4d, we observed the distribution of PRK6 in *raba4d* pollen tubes (Figure 3, A–F; Supplemental Movies S5 and S6). The polar localization of PRK6 was altered in this mutant, with a significantly reduced distribution in the apical membrane-proximal region and the subapical cytoplasm, whereas the distribution of PRK6 at the apical plasma membrane showed no significant difference from the wild-type (Figure 3, B, D–F). Furthermore, *raba4d* pollen tubes did not exhibit an LURE1.2-insensitive phenotype (Figure 3, G and H), perhaps because PRK6 distribution at the apical plasma membrane was still detected in *raba4d* pollen tubes, suggesting that Raba4d mainly affects the polar transport of PRK6 to the pollen tube tip. These findings suggest that ALA3 affects PS-mediated Rab vesicle trafficking at the pollen tube tip and regulates the polar distribution of PRK6 at the pollen tube tip.
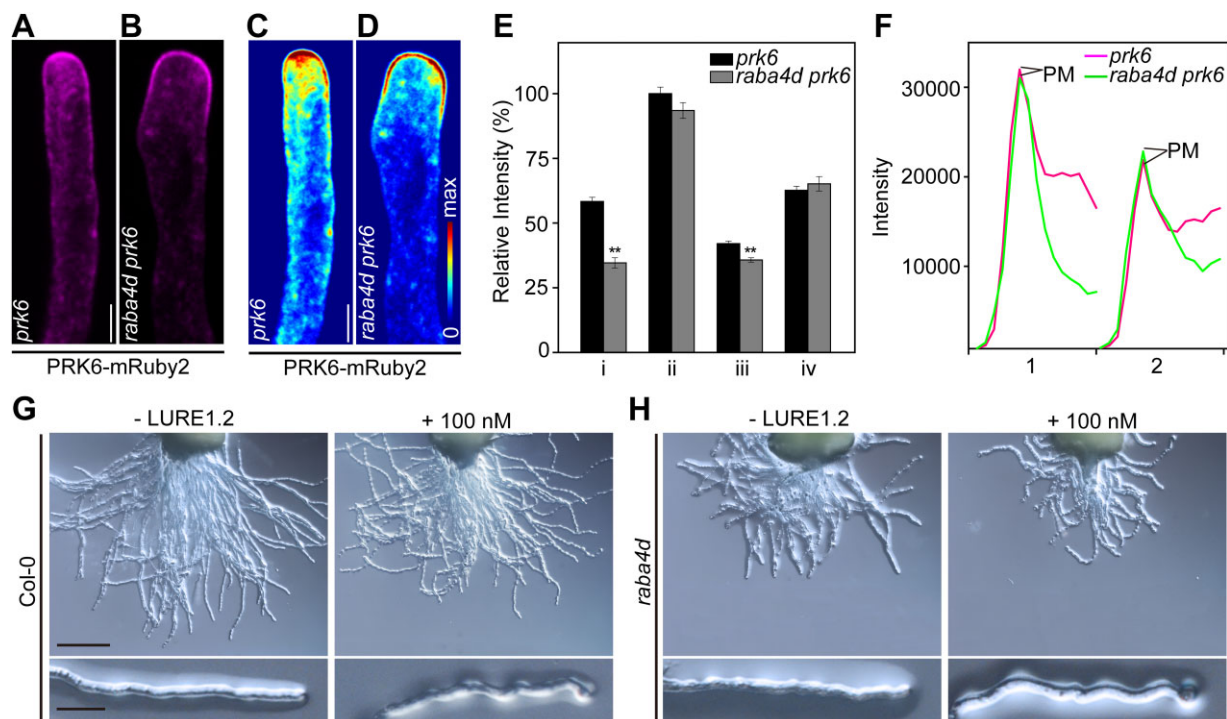
Figure 3 RabA4d is involved in regulating the polar distribution of PRK6 at the pollen tube tip. A–D, Representative confocal images of the pollen tube localization of PRK6–mRuby2 in *prk6* (A) and *raba4d prk6* mutants (B) from the same transgenic line and pseudocolor image of its intensity (C) and (D). Scale bar: 5 μm. E, Quantitative analysis of the relative fluorescence intensity of PRK6–mRuby2 in the apical membrane-proximal region (i), the apical plasma membrane (ii), subapical cytoplasm (iii), and the subapical plasma membrane (iv) shown in Figure 2U. The results represent the means ± SEs (*n* = 30). **$P < 0.01$ (*t* test compared with the wild-type values). F, Plot profile analysis of the changes in the fluorescence signal of PRK6–mRuby2 at the (1) and (2) positions indicated by arrows in Figure 2U. G and H, Semi-in-vivo pollen tube growth/AtLURE1.2-responsive assay of Col-0 (G) and *raba4d* (H). Thirty minutes after pollination, Col-0 and *raba4d* stigmas and styles were excised and incubated for 8 h on semi-in-vivo pollen germination medium containing 0 and 100-nM AtLURE1.2 peptide. The data are representative of at least three independent examinations (*n* = 15). Scale bars: 100 μm (top) and 10 μm (bottom).

Most PRK family members contain polybasic clusters and bind to anionic phospholipids

The subcellular localizations of some membrane proteins or RLKs rely on binding to anionic phospholipids (Yang et al., 2020). Since ALA3 is involved in establishing the polar distribution of PS in pollen tubes (Zhou et al., 2020), we investigated whether PRK family members bind to PS and other anionic phospholipids. We analyzed whether PRK family members contain polybasic clusters (Figure 4A). The polybasic cluster sequence includes three or more contiguous basic amino acids and nearby basic amino acids that together form a cluster with a total number of basic amino acids ≥5. We found that five members of the PRK family (all members except PRK1, PRK5, and PRK7) contain a conserved polybasic cluster in the intracellular JM domain. PRK3 and PRK6 contain a nonconserved polybasic cluster in another site of the intracellular JM domain where the polybasic cluster of PRK1 is also situated (Figure 4A).

To examine whether PRKs bind to anionic phospholipids in vitro, we expressed and purified the recombinant protein of each cytosolic domain of PRKs and mutated PRKs and performed a lipid overlay experiment using the PtdIns(4,5)P2-specific binding protein GST-PLC-1δ PH domain as a positive control (Figure 4C) and GST as a negative control (Figure 4D). GST-cyto-PRK6 mainly bound to PA and PS (Figure 4E). GST-cyto-PRK6^6Q, in which the basic amino acids of the conserved polybasic cluster were mutated, only bound to PA (Figure 4F), and GST-cyto-PRK6^8Q, in which the basic amino acids of the nonconserved polybasic cluster were mutated, slightly bound to PA and PS (Figure 4G; Supplemental Figure S3C). GST-cyto-PRK3 mainly bound to PA and PS but weakly bound to PtdIns(3)P (Figure 4H). GST-cyto-PRK3^8Q (in which the basic amino acids of the conserved polybasic cluster were mutated) and GST-cyto-PRK3^9Q (in which the basic amino acids of the nonconserved polybasic cluster were mutated) could not bind to PS, and the ability of GST-cyto-PRK3^8Q to bind PA was significantly reduced (Figure 4, I and J; Supplemental Figure S3D). GST-cyto-PRK2 mainly bound to PS and PA but weakly bound to PtdIns(3)P (Figure 4M; Supplemental Figure S3G). GST-cyto-PRK1 (Figure 4K; Supplemental Figure S3E) and GST-cyto-PRK8 (Figure 4R; Supplemental Figure S3F) bound to multiple anionic phospholipids and firmly bound to PA, PS and PtdIns(3)P. Mutant forms of GST-cyto-PRK1^11Q (Figure 4L), GST-cyto-PRK2^6Q (Figure 4N), and GST-cyto-PRK8^13Q (Figure 4S) only bound to PA. GST-cyto-PRK4 only bound to PA (Figure 4O), and its
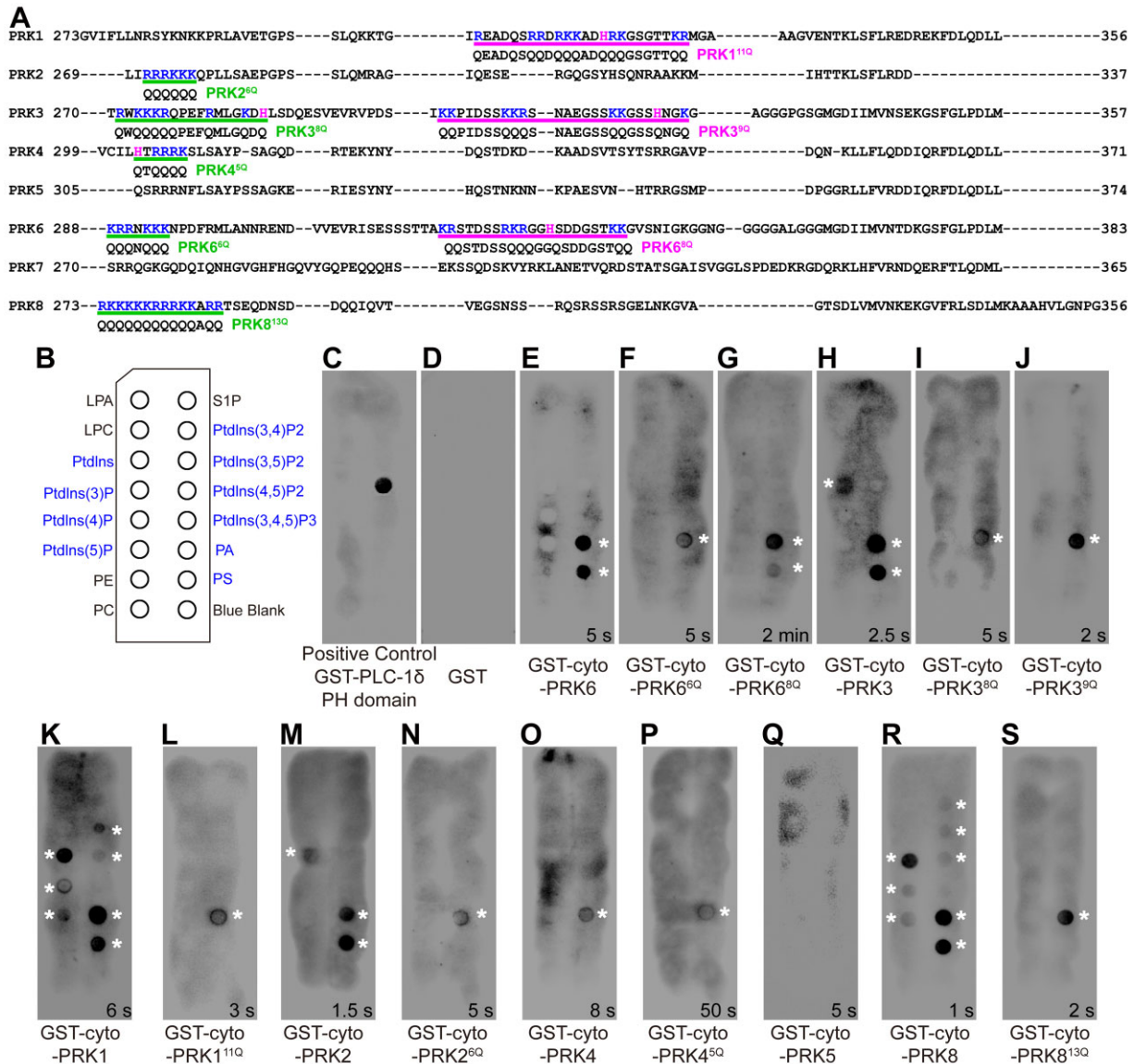
Figure 4 Some members of the PRK family directly bind to multiple anionic phospholipids in vitro. A, Alignment of the intracellular JM domain sequences of PRK1, PRK2, PRK3, PRK4, PRK5, PRK6, PRK7, and PRK8. The basic amino acids arginine (R), lysine (K), and histidine (H) are marked. The conserved polybasic cluster is marked in green, and the nonconserved polybasic cluster is marked in magenta. B, The scheme on the left shows the positions of the different lipids spotted on the membrane: lysophosphatidic acid (LPA), lysophosphocholine (LPC), phosphatidylinositol (PtdIns), phosphatidylinositol-3-phosphate (PtdIns(3)P), phosphatidylinositol-4-phosphate (PtdIns(4)P), phosphatidylinositol-5-phosphate (PtdIns(5)P), phosphatidylethanolamine (PE), phosphatidylcholine (PC), sphingosine 1-phosphate (S1P), phosphatidylinositol-3,4-bisphosphate (PtdIns(3,4)P2), phosphatidylinositol-3,5-bisphosphate (PtdIns(3,5)P2), phosphatidylinositol-4,5-bisphosphate (PtdIns(4,5)P2), phosphatidylinositol-3,4,5-trisphosphate (PtdIns(3,4,5)P3), phosphatidic acid (PA), PS, and blue blank (mock). Anionic phospholipids are highlighted. C and D, Lipid overlay assays showing the lipid-binding ability of the PtdIns(4,5)P2-specific binding protein GST-PLC-δ1 PH domain (positive control) (C) and GST (negative control) (D) using PIP strips. E−S, Lipid overlay assays showing the lipid-binding ability of recombinant GST-cyto-PRK6 (E), GST-cyto-PRK6^6Q (F), GST-cyto-PRK6^8Q (G), GST-cyto-PRK3 (H), GST-cyto-PRK3^8Q (I), GST-cyto-PRK3^9Q (J), GST-cyto-PRK1 (K), GST-cyto-PRK1^11Q (L), GST-cyto-PRK2 (M), GST-cyto-PRK2^6Q (N), GST-cyto-PRK4 (O), GST-cyto-PRK4^5Q (P), GST-cyto-PRK5 (Q), GST-cyto-PRK8 (R), and GST-cyto-PRK8^13Q (S) using PIP strips. The asterisks indicate interactions between recombinant proteins and anionic phospholipids.

mutant form, GST-cyto-PRK4^5Q, exhibited significantly reduced binding to PA (Figure 4P; Supplemental Figure S3H). PRK5 did not bind to any anionic phospholipids (Figure 4Q). These results demonstrate that PRK family members with polybasic clusters bind to anionic phospholipids, but the binding patterns of phospholipids are distinct.

We crossed transgenic lines harboring mCITRINE-C2^Lact-labeled PS with PRK6–mRuby2 transgenic lines for colocalization analysis (Supplemental Figure S3, A and B). Pearson correlation coefficient and kymographic analyses demonstrated that mCITRINE-C2^Lact colocalized to a high degree with PRK6–mRuby2. These results suggest that the polar
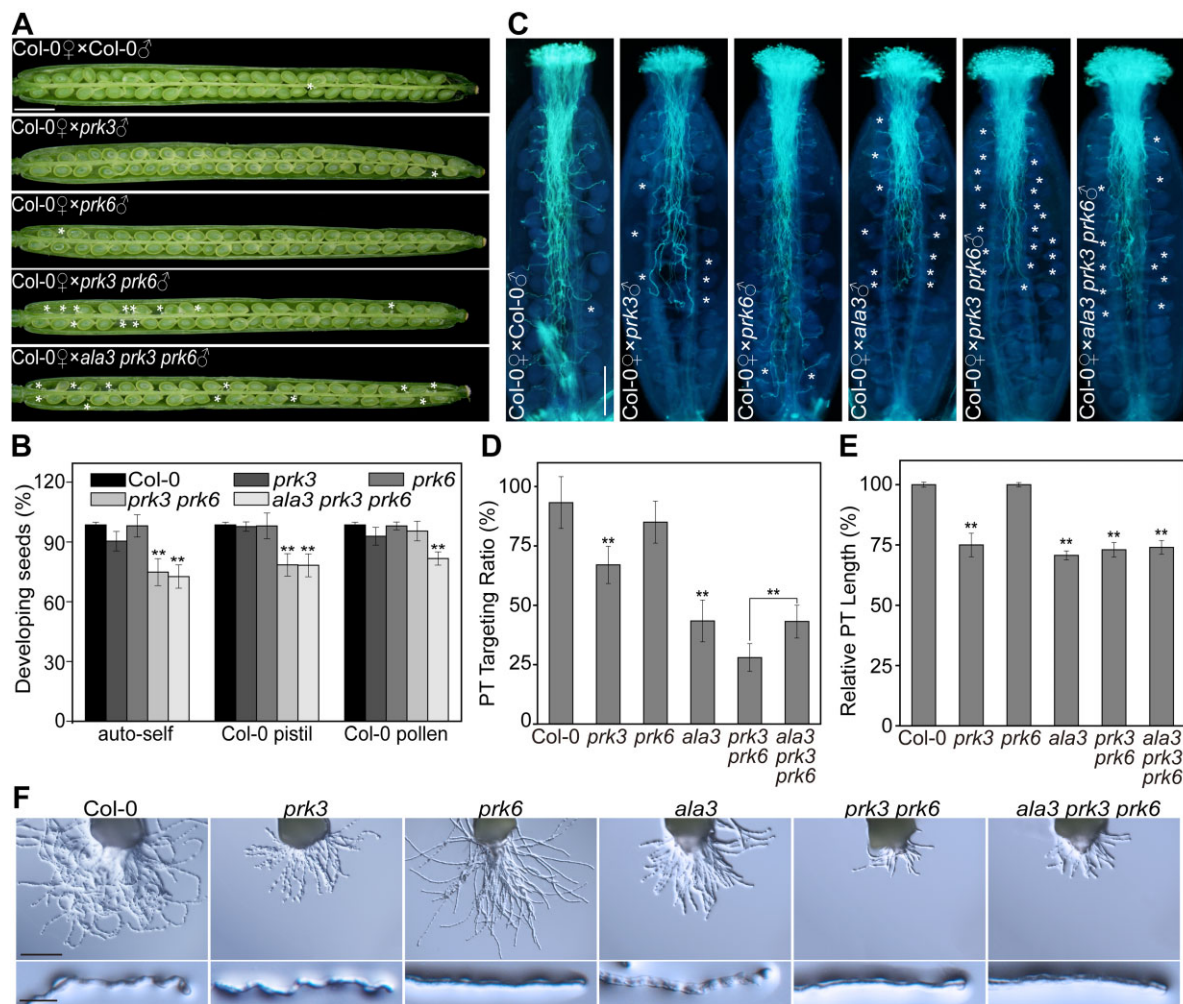
Figure 5 ALA3 likely cooperates with PRK3 and PRK6 to regulate pollen tube growth and guidance. A, Developing seeds in siliques 10 days after pollination of Col-0 with Col-0, *prk3*, *prk6*, *prk3 prk6*, and *ala3 prk3 prk6* pollen. The images are representative of 15 samples. The asterisks indicate white unfertilized ovules, which were counted as aborted seeds. Scale bar: 1 mm. B, Statistical analysis of developing seeds in (A). Three independent examinations were conducted. The data are presented as the mean ± SDs ($n = 15$). **$P < 0.01$ (t test compared with the wild-type values). C, Pollen tubes of Col-0, *prk3*, *prk6*, *ala3*, *prk3 prk6*, and *ala3 prk3 prk6* growing in Col-0 pistils. Aniline blue staining was performed at 8 HAP. The asterisks mark ovules that did not attract nearby pollen tubes. The data are representative of 15 samples for each genotype. Scale bar: 100 μm. D, E, Statistical analysis of the pollen tube (PT) targeting ratio (%) = (targeted ovule number/total number of ovules in pollen tube growth area) * 100% (D) and length of pollen tubes (E) in (C). Three independent examinations were performed. The data are presented as the mean ± SDs ($n = 15$). **$P < 0.01$ (t test compared to the wild-type values). F, Semi-in-vivo pollen tube growth/AtLURE1.2-responsive assay of Col-0, *prk3*, *prk6*, *ala3*, *prk3 prk6*, and *ala3 prk3 prk6*. Thirty minutes after pollination, Col-0, *prk3* and *prk6* stigmas and styles were excised and incubated for 8 h; 1 HAP, *ala3*, *prk3 prk6*, and *ala3 prk3 prk6* stigmas-styles were excised and incubated for 10 h on semi-in-vivo solid pollen germination medium containing 100-nM AtLURE1.2 peptide. The data are representative of at least three independent examinations ($n = 15$). Scale bars: 100 μm (top) and 10 μm (bottom).

localization of PS maintained by ALA3 and other anionic phospholipids is involved in regulating the polar localization of some members of the PRK family at the pollen tube tip.

ALA3 and PRK3/6 genetically regulate pollen tube growth and guidance

Among the members of the PRK family, only PRK3 and PRK6 exhibited particular localization at the tip of the pollen tube, and their subcellular localization patterns were markedly altered in the *ala3* mutant. In addition, the in vivo

phenotypes of growing pollen tubes of the *prk3 prk6* double mutant were comparable to those of the *ala3* mutant (Takeuchi and Higashiyama, 2016; Figure 1). Therefore, we explored whether *ALA3* is genetically related to *PRK3* and *PRK6*. The reciprocal cross experiment showed that the number of seeds set in siliques was significantly lower in *ala3 prk3 prk6* triple mutants when the triple mutants were used as the male or female parent (Figure 5, A and B). In vivo aniline blue staining of the growing pollen tubes of *ala3 prk3 prk6* mutants showed slow growth and impaired

ovule targeting (Figure 5, C–E). The semi-in-vivo results showed that the pollen tubes of the *ala3 prk3 prk6* triple mutants exhibited insensitivity to LURE1.2 and slow growth (Figure 5F). However, these phenotypes exhibited by the *ala3 prk3 prk6* triple mutants were not aggravated compared with those of the *ala3* mutant and *prk3 prk6* double mutants (Figure 5). In conclusion, the abortion and pollen tube-related phenotypes of *ala3* mutants are partially caused by the effects of *PRK3* and *PRK6*, which might function in the same genetic pathway.

The binding of PRK3 and PRK6 to phospholipids is critical for their subcellular localization

According to the above-described conclusions, the PRK3/6 mutant forms show defects in binding to phospholipids such as PS and PA. To determine the effects of phospholipids on the polar distribution of PRK3 and PRK6 at the pollen tube tip, we created transgenic rescued plants with mutations in the polybasic clusters of PRK6 and PRK3. Mutations in different polybasic clusters affected their localization patterns to varying degrees. Compared with tip-localized PRK6–GFP (Figure 6, A, D, and E; Supplemental Movie S7), the distribution of PRK6^{6Q}–GFP at the apical membrane-proximal region, the apical plasma membrane, and the subapical plasma membrane of the pollen tube was reduced in the *prk6* mutant, and the fluorescence signals extended to the shank plasma membrane (Figure 6, B, D, and F; Supplemental Movie S8). The distribution of PRK6^{8Q}–GFP in the apical membrane-proximal region, the apical plasma membrane and the subapical plasma membrane of *prk6* pollen tube was also significantly reduced, showing a shank plasma membrane localization pattern (Figure 6, C, D, and G; Supplemental Movie S9). The preferential localization of PRK6 at the plasma membrane was caused by mutations within the polybasic clusters, which destroyed the pattern of polar distribution at the pollen tube tip (Figure 6D).

Compared with tip-localized PRK3–GFP (Figure 6, H, K, and L; Supplemental Movie S10), the distribution of PRK3^{8Q}–GFP at the apical membrane-proximal region, the apical plasma membrane, and the subapical plasma membrane was significantly reduced in *prk3 prk6* pollen tubes, and the fluorescence signals in the shank plasma membrane and the shank cytoplasm of pollen tubes were more apparent (Figure 6, I, K, and M; Supplemental Movie S11). The distribution of PRK3^{9Q}–GFP in the apical plasma membrane and the subapical plasma membrane of *prk3 prk6* pollen tubes was also significantly reduced, and the fluorescence signals in the shank plasma membrane and the shank cytoplasm of *prk3 prk6* pollen tubes increased (Figure 6, J, K, and N; Supplemental Movie S12). Thus, the polybasic cluster mutation in PRK3 led to the mislocalization of this protein in the shank plasma membrane and organelles without maintaining the normal apical polar localization (Figure 6K). These results suggest that anionic phospholipids such as PS and PA are directly involved in regulating the precise localization of PRK3 and PRK6.

Mutated *PRK3* and *PRK6* do not fully rescue the phenotypes of *prk* mutants

We investigated the impact of PRK3 and PRK6 with different polybasic cluster mutations on physiological functions. We examined whether *PRK3–GFP*, *PRK3^{8Q}–GFP*, and *PRK3^{9Q}–GFP* could rescue the abortion and slow pollen tube growth of the *prk3 prk6* mutant and whether *PRK6–GFP*, *PRK6^{6Q}–GFP*, and *PRK6^{8Q}–GFP* could rescue the defects in ovule targeting and insensitivity to LURE1.2 of the *prk6* mutant. In a reciprocal cross experiment, the percentage of developing seeds/total number of seeds in siliques was approximately 98%, 91%, 79%, and 87% in wild-type, *PRK3–GFP*, *PRK3^{8Q}–GFP*, and *PRK3^{9Q}–GFP*, respectively, when these mutants were used as the male parents (Figure 7, A and B).

We observed the in vivo pollen tube growth rate by aniline blue staining. When the wild-type was used as the female parent, *PRK3–GFP* pollen tubes approached the bottom of the pistil, *PRK3^{8Q}–GFP* pollen tubes reached the middle of the pistil, and *PRK3^{9Q}–GFP* pollen tubes had grown to two-thirds the length of the pistil 8 h after artificial pollination (Figure 7, C and D). Aniline blue staining showed that *PRK6–GFP* pollen tubes targeted nearby ovules. *PRK6^{6Q}–GFP* and *PRK6^{8Q}–GFP* partially rescued the defect in ovule targeting, but the effect obtained with *PRK6^{6Q}–GFP* was better than that obtained with *PRK6^{8Q}–GFP* (Figure 7, E and F). Consistent with the in vivo results, *PRK3–GFP* rescued the slow growth of *prk3 prk6* pollen tubes, *PRK3^{8Q}–GFP* hardly rescued the defect in pollen tube growth, and *PRK3^{9Q}–GFP* partially rescued the phenotype (Figure 7G). *PRK6–GFP* rescued the ability of the *prk6* pollen tube to perceive AtLURE1.2, and the *PRK6^{6Q}–GFP* and *PRK6^{8Q}–GFP* pollen tubes exhibited partial rescue of the ability to perceive LURE1.2 in the semi-in-vivo system (Figure 7H). These results indicate that the ability of PRK3 and PRK6 to bind anionic phospholipids such as PS and PA is essential for their polar localization in pollen tubes and for the regulation of pollen tube growth and guidance and embryo abortion.

Discussion

The ALA family in *A. thaliana* consists of 12 members, and six ALAs are expressed in pollen (Zhou et al., 2020). Here we found that loss of ALA3 function caused pollen tube defects in growth and micropyle guidance in vivo (Figure 1E) and insensitivity to exogenous AtLURE1.2 secreted by female gametophytes in a semi-in-vivo assay (Figure 5F). We also examined whether similar phenotypes existed in the five remaining *ala* single mutants expressed in pollen. As shown in Supplemental Figure S4, none of the remaining 5 *ala* single mutants exhibited defects in pollen tube guidance. These results indicate that ALA3 plays a major role in the regulation of pollen tube guidance within the Arabidopsis ALA family.
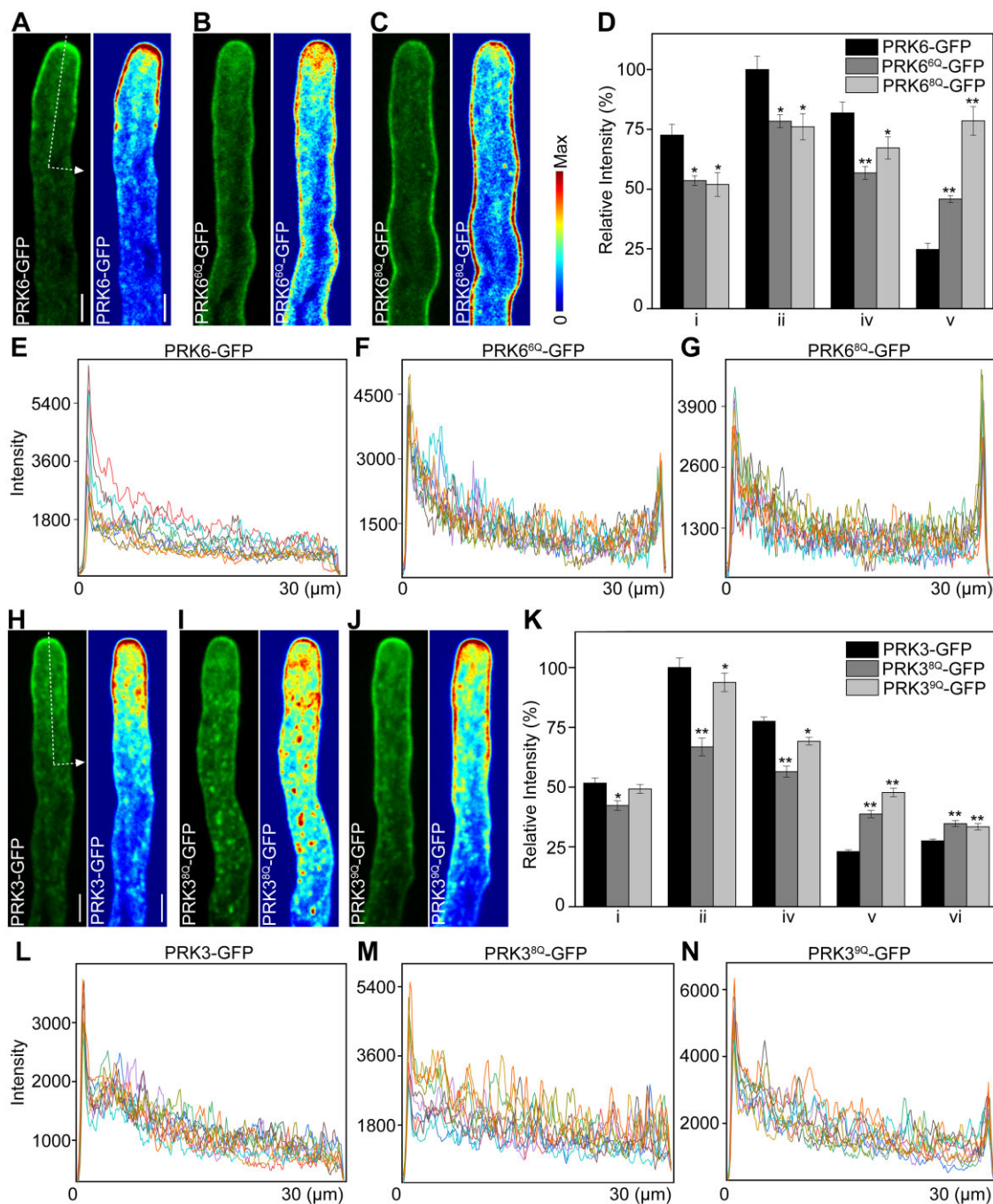
Figure 6 The subcellular localization of mutated PRK3 and PRK6 is significantly altered. A–C, Representative confocal images of the pollen tube localization of PRK6–GFP (A), PRK6^{6Q}–GFP (B), and PRK6^{8Q}–GFP (C) in the *prk6* background. The pseudocolored fluorescence intensity of the images is shown on the right. The data are representative of more than 30 tubes. Scale bar: 5 μm. D, Quantitative analysis of the relative fluorescence intensity of PRK6–GFP (A), PRK6^{6Q}–GFP (B), and PRK6^{8Q}–GFP (C) in the apical membrane-proximal region (i), the apical plasma membrane (ii), the subapical plasma membrane (iv), and the shank plasma membrane (v) shown in Figure 2U. The results are presented as the means ± sEs (n = 30). *P < 0.05; **P < 0.01 (t test compared with the wild-type values). E–G, Plot profile analysis of the changes in the fluorescence signals of PRK6–GFP (E), PRK6^{6Q}–GFP (F), and PRK6^{8Q}–GFP (G) at the arrow (30 μm from the front edge) shown in (A). Data for 10 pollen tube samples were analyzed. H–J, Representative confocal images of the pollen tube localization of PRK3–GFP (H), PRK3^{8Q}–GFP (I), and PRK3^{9Q}–GFP (J) in the *prk3 prk6* background. The pseudocolored fluorescence intensity of the images is shown on the right. The data are representative of more than 30 tubes. Scale bar: 5 μm. K, Quantitative analysis of the relative fluorescence intensity of PRK3–GFP (H), PRK3^{8Q}–GFP (I), and PRK3^{9Q}–GFP (J) in the apical membrane-proximal region (i), the apical plasma membrane (ii), the subapical plasma membrane (iv), the shank plasma membrane (v), and the shank cytoplasm (vi) shown in Figure 2U. The results are presented as the means ± sEs (n = 30). *P < 0.05; **P < 0.01 (t test compared with the wild-type values). L–N, Plot profile analysis of the changes in the fluorescence signals of PRK3–GFP (L), PRK3^{8Q}–GFP (M), and PRK3^{9Q}–GFP (N) at the arrow (30 μm from the front edge) shown in (H). The data for 10 pollen tube samples were analyzed.
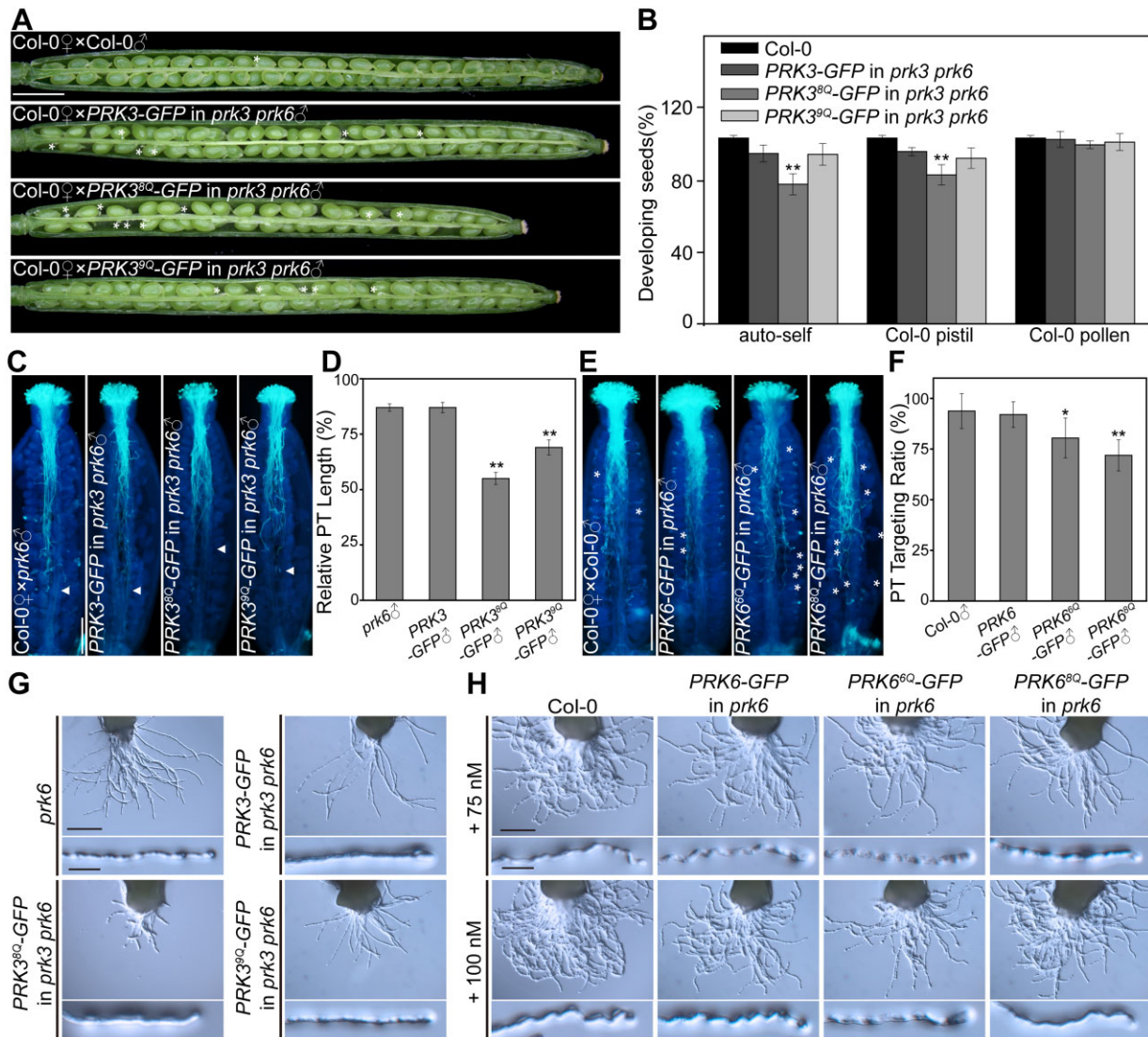
Figure 7 Mutated PRK3 and PRK6 do not effectively restore the phenotype of the *prk3 prk6* and *prk6* mutants. A, Developing seeds in siliques 10 days after pollination of Col-0 with pollen from the *PRK3–GFP*, *PRK3^{8Q}–GFP*, and *PRK3^{9Q}–GFP* complementation transgenic lines. The images are representative of 15 samples. The asterisks indicate white unfertilized ovules, which were counted as aborted seeds. Scale bar: 1 mm. B, Statistical analysis of developing seeds in (A). Three independent examinations were performed. The data are presented as the mean ± SDs ($n = 15$). **$P < 0.01$ (t test compared with the wild-type values). C, E, Pollen tubes of *PRK3–GFP*, *PRK3^{8Q}–GFP*, and *PRK3^{9Q}–GFP* in *prk3 prk6* mutants (C), *PRK6–GFP*, *PRK6^{6Q}–GFP*, and *PRK6^{8Q}–GFP* in *prk6* mutants (E), and complementation transgenic lines growing in Col-0 pistils. Aniline blue staining was performed at 8 HAP. The asterisks mark ovules that did not attract pollen tubes. The arrows indicate the tip of the longest pollen tube in the transmitting tract. The data are representative of 15 samples of each genotype. Scale bar: 100 μm. D, F, Statistical analysis of the length of pollen tubes (D) in (C) and the pollen tube targeting ratio (F) of pollen tubes in (E). Three independent examinations were performed. The data are presented as the mean ± SDs ($n = 15$). **$P < 0.01$ (t test compared with the wild-type values). G, H, Semi-in-vivo pollen tube growth/AtLURE1.2-responsive assay of *PRK3–GFP*, *PRK3^{8Q}–GFP*, and *PRK3^{9Q}–GFP* in *prk3 prk6* mutants (G) and *PRK6–GFP*, *PRK6^{6Q}–GFP*, and *PRK6^{8Q}–GFP* in *prk6* mutants (H). Thirty minutes after pollination, Col-0, *prk6*, *PRK6–GFP*, *PRK6^{6Q}–GFP*, *PRK6^{8Q}–GFP*, *PRK3–GFP*, and *PRK3^{9Q}–GFP* stigmas-styles were excised and incubated for 8 h; 1 HAP, *PRK3^{8Q}–GFP* stigmas-styles were excised and incubated for 10 h on semi-in-vivo solid pollen germination medium containing 75 nM or 100-nM AtLURE1.2 peptide. The data are representative of at least three independent examinations ($n = 15$). Scale bars: 100 μm (top) and 10 μm (bottom).

The defective growth and guidance of *ala3* pollen tubes is due to the changes in the subcellular localization of PRK family members resulting from the functional deficiency of ALA3

PRK family members perceive and bind to different small peptides to participate in multiple signaling pathways in sexual reproduction. Among the members of the Arabidopsis PRK family, only ligands for PRK6 and PRK5 have been reported. PRK5 binds to GRIM REAPER (GRI), which is the homolog of LeSTIG1 in Arabidopsis, and triggers cell death in a superoxide-dependent manner (Wrzaczek et al., 2009), but its role in pollen tubes is

unknown. The extracellular domain of PRK6 is specifically bound by AtLURE1.2 to further activate the ovule-targeting signaling pathway of pollen tubes (Takeuchi and Higashiyama, 2016). The *prk3 prk6*, *prk1 prk3 prk6*, and *prk3 prk6 prk8* mutants exhibited marked reductions in pollen tube growth and fertility (Takeuchi and Higashiyama, 2016), but the small peptides involved in their regulation of pollen tube growth are unclear.

Each PRK family member contains a transmembrane domain, but their subcellular localizations vary. For example, PRK3 and PRK6 were not evenly distributed on the plasma membrane of the pollen tubes but primarily localized to the apical plasma membrane and in the apical membrane-proximal region of the pollen tubes (Takeuchi and Higashiyama, 2016; Figure 2, A–J). The localization of PRK6 at the pollen tube tip was asymmetrically distributed toward the direction of exogenous AtLURE1.2, which resulted in remodeling of the tip localization of PRK6 (Takeuchi and Higashiyama, 2016). PRK1 was mainly distributed in the apical plasma membrane, the shank plasma membrane and the apical inverted-cone zone (Figure 2, K–O). In contrast, PRK2, PRK4, PRK5, and PRK8 had weak signals at the pollen tube tip and were mainly distributed on the shank plasma membrane (Zhao et al., 2013; Wrzaczek et al., 2015; Duckney et al., 2017; Supplemental Figure S2; Figure 1, P–T).

Because pollen tubes are typical polar-growing cells in which elongation occurs only in the apical region (Hepler et al., 2001; Cheung and Wu, 2008), the establishment and maintenance of the polar distribution of PRK6 and other PRKs in tips may be vital for the regulation of pollen tube growth and guidance toward ovules. We revealed that the localization patterns of PRK3 and PRK6 were significantly altered in the *ala3* mutant. The distribution of PRK6 and PRK3 was markedly reduced in the apical plasma membrane and apical membrane-proximal region in *ala3* pollen tubes and aggregated on two sides of the subapical cytoplasm. The fluorescence signals of PRK6–mRuby2 increased in the subapical plasma membrane (Figure 2, A–J). The distribution of PRK1, PRK4, and PRK8 in the apical membrane-proximal region of *ala3* pollen tube was also reduced (Figure 2, O and T; Supplemental Figure S2N). Genetic analysis revealed that the pollen tubes of the *ala3 prk3 prk6* triple mutant did not exhibit an exacerbated growth and guidance phenotype compared to the *ala3* single and *prk3 prk6* double mutants (Figure 5). Therefore, we hypothesize that the loss of ALA3 function affects the precise localization of PRK1, PRK3, PRK6, and PRK8 in pollen tubes, which induces defects in pollen tube growth and guidance in *ala3* mutants.

ALA3 regulates the polar distribution of PRK6 at the pollen tube tip via RabA4d-mediated vesicle trafficking

The process underlying the polar distribution of proteins depends on the establishment and maintenance of directional transport. The endomembrane system is needed for the directional transport of proteins to specific sites, the strong accumulation of proteins, and further recycling by endocytosis and redistribution between the trans-Golgi network/endosome and plasma membrane (Yang et al., 2020; Dubois and Jaillais, 2021; Hou et al., 2021; Ruan et al., 2021). Phospholipid transport catalyzed by P4-ATPase plays an important role in vesicle transport. In budding yeast (*Saccharomyces cerevisiae*), *drs2p* and *neo1*, two mutants of P4-ATPases family members, show a loss of Golgi membrane curvature and defects in protein transport (Chen et al., 1999; Hua and Graham, 2003). The recruitment of EHD1 (Eps15 homology domain-containing protein 1) to recycling endosomes is dependent on the PS flippase activity of ATP8A1 and ATP8A2, which are mammalian orthologs of Drs2 (Lee et al., 2015). The absence of TAT-5, the nematode (*Caenorhabditis elegans*) homolog of Drs2, results in considerable shedding of plasma membrane-derived extracellular vesicles (Wehman et al., 2011; Beer et al., 2018). P4-ATPase also participates in coat protein complex I- (Hua et al., 2002; Xu et al., 2017), clathrin-, adaptor- (Chen et al., 1999; Liu et al., 2008; Schultzhaus et al., 2015; Martzoukou et al., 2017), and retromer-dependent trafficking routes (Wu et al., 2016; Dalton et al., 2017; McGough et al., 2018).

Furthermore, transmission electron microscopy revealed a significant trans-Golgi stacking and secretory vesicle formation defect at peripheral columellar cells of the root tip in Arabidopsis *ala3* mutants (Poulsen et al., 2008). Trichome development and pollen tube growth, which depend on polar endosomal trafficking, are also impaired in *ala3* mutants (Zhang and Oppenheimer, 2009; McDowell et al., 2013). The *ala3* mutants also show defects in polar trafficking of the ATP-binding cassette (ABC) transporter protein PENETRATION 3 (PEN3) and the soluble N-ethylmaleimide sensitive factor attachment protein receptor (SNARE) protein PEN1; PEN3 and PEN1 are needed to establish an effective defense against numerous fungal pathogen invasions (Underwood et al., 2017). The *ala3* mutants show defects in the asymmetric distribution of auxin and the polar trafficking of the auxin transporter PIN; moreover, the quintuple mutant *ala3/4/5/9/11* and the sextuple mutant *ala3/4/5/9/10/11* also display a lack of gravitropic response and PIN trafficking and polarity (Zhang et al., 2020). Arabidopsis ALA1 and ALA7 are responsible for the cellular detoxification of fungal toxins. Detoxification is achieved through ALA1-/ALA7-mediated vesicular trafficking, which transports the toxins from the plasma membrane to vesicles for degradation (Wang et al., 2021). These observations suggest that ALA proteins play a crucial role in the maintenance of polarity and endosomal trafficking.

We previously demonstrated that the loss of ALA3 function affects the polar distribution of PS, as well as PS-mediated secretion-associated RabA4d and recycling-associated RabA1e and RabA1g at the pollen tube tip, which influence secretion-associated endomembrane transport processes (Zhou et al., 2020). We also found that the distribution of PRKs in the apical vesicle-rich inverted-cone zone was reduced to different levels in the pollen tube tips of the *ala3* mutants. The polar localization of PRK6 was altered in

raba4d mutant pollen tubes, mainly due to decreased distribution in the inverted cone zone, but was not significantly altered at the apical plasma membrane (Figure 3, A–F), which suggests that the loss of ALA3 function affects PS-mediated RabA4d vesicle trafficking to regulate the polar distribution of PRK6 at the pollen tube tip. In addition, PRK1 was recently used as a marker for detecting the secretory pathway of pollen tubes, and the apical localization of PRK1 is dependent on the secretory pathway (Guo and Yang, 2020; Wang et al., 2020), which suggests that ALA3 also affects the distribution of PRKs by influencing polar transport mediated by secretory vesicles at the pollen tube tip.

Anionic phospholipids are essential for the subcellular localization of PRKs

Anionic phospholipids control the localization and functions of proteins by affecting the surface charge, curvature, and lipid packing of the membrane and the recruitment of effector proteins and associated phospholipid-binding proteins (Di Paolo and De Camilli, 2006; Yeung et al., 2008; Bigay and Antonny, 2012; Xu et al., 2013). Anionic phospholipids exhibit different subcellular localization patterns and functions in pollen tubes. PS is mainly distributed in the apical vesicle-rich inverted cone zone and apical plasma membrane (Zhou et al., 2020; López-Marqués, 2021). Late endosome/multivesicular body-localized PtdIns(3)P is involved in vesicle degradation (Vermeer et al., 2006). PtdIns(4)P mainly accumulates at the subapical and shank plasma membrane (Zhao et al., 2010). PtdIns(4,5)P2 is mainly localized to the apical and subapical plasma membranes (Kost et al., 1999; Hempel et al., 2017), and PA is a plasma membrane-localized lipid in tobacco (*Nicotiana tabacum*) pollen tubes (Potocký et al., 2014). The loss of ALA3 function resulted in the failure of PS to effectively flip to the cytoplasmic side of the plasma membrane and organelles to localize at the pollen tube tip and a marked decline in pollen tube growth (Zhou et al., 2020).

Here, sequence analysis revealed that six members of the Arabidopsis PRK family (all members except PRK5 and PRK7) contain one or two polybasic clusters in the intracellular JM domain and are capable of binding various types of anionic phospholipids in vitro (Figure 4). However, different PRKs have different binding capacities to different types of phospholipids. Mutations of polybasic clusters in the JM domain significantly decreased the ability of PRKs to bind anionic phospholipids in vitro. PRK3 and PRK6 mutations in the polybasic clusters did not effectively rescue the pollen tube growth deficiency of the *prk3 prk6* mutant or the pollen tube guidance deficiency of the *prk6* mutant (Figure 7). PRK6^{6Q}, PRK6^{8Q}, PRK3^{8Q}, and PRK3^{9Q} exhibited a significantly reduced ability to bind PS in vitro or were unable to bind PS, and a marked alteration in their localization pattern in pollen tubes was observed (Figure 6). These proteins showed significantly decreased levels in the apical inverted-cone and membrane-proximal regions, where PS was abundantly distributed, but were heavily aggregated throughout

the pollen tube plasma membrane or organelles (Figure 6, D and K). These results support the hypothesis that the subcellular localization and functions of PRK3 and PRK6 in pollen tube tips depend on their combination with anionic phospholipids.

We analyzed the amino acid sequences of 223 Arabidopsis LRR-RLK family members and discovered that 93 LRR-RLK members contained conserved polybasic clusters, 4 LRR-RLK members contained nonconserved polybasic clusters similar to PRK1, and 6 LRR-RLK members, resembling PRK3/6, contained two polybasic clusters (Supplemental Data Set S1). These results suggest that polybasic clusters may be critical for the proper localization of several RLKs. In addition, multiple recent studies have suggested that anionic phospholipids are involved in the coordination of protein localization and function. For example, the auxin transport regulator PINOID (PID), the brassinosteroid receptor kinase BRI1 KINASE INHIBITOR1 (BKI1) and another family member, MAKR1-4, bind to anionic phospholipids in plants, which requires the targeting of a polybasic unstructured loop to the plasma membrane (Jaillais et al., 2011; Barbosa and Schwechheimer, 2014; Simon et al., 2016; Hempel et al., 2017). The localization of many mammalian proteins in the plasma membrane also relies on a cluster of cationic residues (Kost et al., 1999; Heo et al., 2006). Therefore, combining with anionic phospholipids is indispensable for the subcellular localization and functions of many proteins.

The polar distribution of PRKs is likely influenced by their C-termini

Notably, the transmembrane domain of PRK2 was not essential for its localization to the shank plasma membrane. Functional site deletion experiments demonstrated that PRK2 with a deletion of the JM domain showed a punctiform localization pattern at the shank plasma membrane; in addition, PRK2 with deletion of the C-terminal domain localized to the plasma membrane, but its localization at the apical plasma membrane of the pollen tube was more concentrated than that of wild-type PRK2. The deletion of both the JM domain and the C-terminal domain in PRK2 rendered the protein unable to localize to the plasma membrane and instead mislocalized to the motor vesicles of the pollen tube shank. Moreover, the plasma membrane localization of PRK2 was unaffected by its kinase activity. These results indicate that the JM domain and C-terminal domain, but not the TM domain, are crucial for PRK2 localization (Zhao et al., 2013).

The JM domain of PRK5 lacks the polybasic cluster (Figure 4A). PRK5 cannot bind to anionic phospholipids in vitro (Figure 4Q), but its primary localization was on the shank plasma membrane (Supplemental Figure S2, I and J). Sequence analysis revealed that only PRK3 and PRK6 in the Arabidopsis PRK family lack a carboxy-terminal domain (Supplemental Figure S5), whereas PRK2/4/5/8, which contain carboxy-terminal domains, primarily localized to the shank plasma membrane, and the carboxy-terminal domain

may be indispensable for the localization of PRK5. We propose that PRK3 and PRK6 are more easily recruited by PS to the tip of the pollen tube because the carboxy-terminal domain has no influence on PRK localization. However, the mechanism through which the C-terminal domain regulates PRK localization in the shank plasma membrane is unclear.

Therefore, the localization of PRKs appears to be a complex, precisely regulated process that requires the engagement of various signaling molecules and effector proteins. PS may synergistically regulate the polar distribution of PRKs at the pollen tube tip by directly recruiting and indirectly influencing PS-mediated endomembrane transport. Further research on the precise localization of PRKs is needed.

Materials and methods

Plant materials
Arabidopsis thaliana ecotype Columbia-0 (Col-0) was used as the wild-type. Seeds of the T-DNA insertions *ala3* (SALK_082157), *raba4d* (CS360297), *ala1* (SALK_056947), *ala6* (SALK_150173), *ala7* (SALK_125598), *ala9* (SALK_128495), and *ala12* (SALK_111498) were obtained from the Arabidopsis Biological Resource Center (ABRC). These mutant lines were previously reported (Zhou et al., 2020). The transgenic line *pUBQ10-mCITRINE-C2^{Lact}* (NASC# N2107347; Platre et al., 2018) was provided by the Nottingham Arabidopsis Stock Centre (NASC). Previously published Arabidopsis lines were used in this study included *prk6* (SALK_129244C), *prk3* (FLAG_540B08), *pPRK3–PRK3–mClover*, and *pPRK6–PRK6–mRuby2* (Takeuchi and Higashiyama, 2016). The T-DNA insertions were identified by genomic PCR as described previously (Zhou et al., 2020), and all primers used for genotypic PCR are listed in Supplemental Table S1.

Plant growth conditions
All seeds were vernalized for 3 days at 4°C, sown on Murashige and Skoog medium (MS, PhytoTech M519) containing 2% (w/v) sucrose and 0.8% (w/v) agar, and incubated for 7 days at 23°C under a 16-h light/8-h dark cycle. The seedlings were transferred to soil and grown in a greenhouse at 23°C under a 16-h light/8-h dark cycle at an optical density of 100 μmol m^{-2} s^{-1} (bulb type, TCL, TCLMY-28) and 65% relative humidity.

Plasmid construction and plant transformation
To generate the *pBIB–HYG–pALA3–ALA3–HA* construct for complementation, the sequences of the 2,000-bp promoter and 2,143-bp genome regions of *ALA3* were amplified by PCR using total Arabidopsis genomic DNA as the template. The amplified segments were cloned into the reconstructed vector *pBIB–HYG–pALA3–GWR–HA* through the *pDONR/zeo* (Invitrogen) vector using BP Clonase (Invitrogen) and subsequently LR Clonase (Invitrogen).

To generate the *pGWB4–HYG–pPRK6–PRK6–GFP* construct for subcellular localization analysis and complementation, the sequences of the 856-bp promoter and 2,096-bp genomic regions of *PRK6* were amplified by PCR using total Arabidopsis genomic DNA as the template. The amplified segments were cloned and inserted into the destination vector *pGWB4–HYG–GWR–GFP* using BP and LR Clonase. The same promoter sequence of *PRK6* was cloned, and PRK6 proteins with point mutations (PRK6^{6Q} and PRK6^{8Q}) were generated via gene synthesis to generate the constructs *pGWB4–HYG–pPRK6–PRK6^{6Q}–GFP* and *pGWB4–HYG–pPRK6–PRK6^{8Q}–GFP*, respectively.

The sequences of the 807-bp promoter and 1,988-bp genomic regions of *PRK3* were amplified by PCR using the total Arabidopsis genomic DNA as the template to generate the construct *pGWB4–HYG–pPRK3–PRK3–GFP*. The same promoter sequence of *PRK3* was cloned, and PRK3 proteins with point mutations (PRK3^{8Q} and PRK3^{9Q}) were generated via gene synthesis to generate the constructs *pGWB4–HYG–pPRK3–PRK3^{8Q}–GFP* and *pGWB4–HYG–pPRK3–PRK3^{9Q}–GFP*, respectively.

The sequences of the 624-bp promoter and 2,056-bp genomic regions of *PRK1* were amplified by PCR using total Arabidopsis genomic DNA as the template to generate the construct *pGWB4–HYG–pPRK1–PRK1–GFP*. The sequences of the 1,155-bp promoter and 2,213-bp genomic regions of *PRK4* were amplified by PCR using total Arabidopsis genomic DNA as the template to generate the construct *pGWB4–HYG–pPRK4–PRK4–GFP*.

The sequences of the 2,212-bp promoter and 2328-bp genomic regions of *PRK5* were amplified by PCR using total Arabidopsis genomic DNA as the template to generate the construct *pGWB4–HYG–pPRK5–PRK5–GFP*. The sequences of the 2,259-bp promoter and 2,021-bp genomic regions of *PRK8* were amplified by PCR using total Arabidopsis genomic DNA as the template to generate the construct *pGWB4–HYG–pPRK8–PRK8–GFP*.

All PCR amplifications were performed using Q5U Hot Start High-Fidelity DNA Polymerase (New England Biolabs). Sequencing analyses were performed to confirm the amplified fragments. The primers used for the cloning experiments are described in Supplemental Table S1. Four-week-old plants were transformed with *Agrobacterium tumefaciens* (strain GV3101) using the floral dip method as described previously (Clough and Bent, 1998). The transgenic plants were selected using hygromycin.

Aniline blue staining
The stamens of stage 12 flowers were detasseled, and pollen grains from stage 13 flowers from wild-type or mutant plants were dabbed onto stigma papillar cells after 12–16 h. Pistils were excised 8 and 17 HAP, fixed, rehydrated, softened, and stained with 0.1% decolorized aniline blue as described previously (Zhou et al., 2020). The stained samples were observed under a fluorescence microscope (Olympus BX53, Japan) equipped with a UV filter set.

Scanning electron microscopy
The pistils were excised from flowers 17 HAP and fixed in FAA solution (50% ethanol, 5% acetic acid, and 3.7%

formaldehyde) for more than 24 h. The fixed pistils were dehydrated through a graded ethanol series and an isoamyl acetate series as described previously (Guo et al., 2009). The pistils were dried at the CO_2 critical point (Leica EM CPD300) and placed on the stage for further dissection. After sputter coating with gold, the samples were observed under a scanning electron microscope (JOEL JSM-IT500LA).

Semi-in-vivo pollen tube growth and AtLURE1-responsive assay

The recombinant His-tagged AtLURE1.2 peptide was expressed in *Escherichia coli* BL21, purified, and refolded as described previously (Liu et al., 2013; Wang et al., 2016). For the AtLURE1.2-responsive wavy assay, the semi-in-vivo pollen germination medium (14% sucrose, 0.001% boric acid, 1.27-mM $Ca(NO_3)_2$, 0.4-mM $MgSO_4$, and 1.5% ultralow gelling temperature agarose (HydraGene); adjusted to pH 7.0 with KOH) was melted, and the purified AtLURE1.2 peptide was added to the solid medium after cooling to 40°C –50°C. The mixture was mixed uniformly by vortexing. A certain amount was added to the glass slides under moist conditions. Thirty minutes to 1 HAP, wild-type stigma-styles were excised using an operating knife under a dissecting microscope, rapidly transferred to semi-in vivo solid pollen germination medium and incubated at 22°C for 8–10 h. Images were obtained using a ZEN2 microscope equipped with ZEN 2.3 software (Carl Zeiss).

Confocal microscopy and image analysis

Confocal images of growing pollen tubes were obtained using a spinning-disk confocal microscope equipped with an iXON ultra EMCCD camera (Andor) as previously reported (Zhou et al., 2020). A 63× NA oil immersion lens was used to observe the samples. Andor IQ3 software was used for image acquisition. Time-lapse images were captured every 0.5 s to 5 s for 30 s to 5 min. The excitation/emission wavelengths were, respectively, 488 nm/514 nm for GFP and mClover, 514 nm/542 nm for YFP and mCitrine, and 561 nm/607 nm for mRuby2. The images were quantified using ImageJ software. To evaluate colocalization, Pearson correlation coefficients were calculated using ImageJ with the Colocalization Finder plugin, and Fiji with the Kymograph plugin was used to produce kymographs.

Protein expression, purification, and lipid overlay assay

Sequences encoding the cytosolic domains (cyto-) of PRK1, PRK2, PRK3, PRK4, PRK5, PRK6, and PRK8 were amplified from the Col-0 cDNA library using the primers listed in Supplemental Table S1. The PCR products were cloned into the pMD19-T vector and the pGEX4T-1 destination vector. For protein expression, the expression plasmids were transformed into *E. coli* Rosetta cells. GST-tagged recombinant proteins were purified as previously described (Xiang et al., 2007). Cyto-PRKs with point mutations (PRK1[11Q], PRK2[6Q], PRK3[8Q], PRK3[9Q], PRK4[5Q], PRK6[6Q], PRK6[8Q], and PRK8[13Q]) were generated via gene synthesis to generate the constructs

GST-cyto-PRK1[11Q], GST-cyto-PRK2[6Q], GST-cyto-PRK3[8Q], GST-cyto-PRK3[9Q], GST-cyto-PRK4[5Q], GST-cyto-PRK6[6Q], GST-cyto-PRK6[8Q], and GST-cyto-PRK8[13Q], respectively. The primers are listed in Supplemental Table S1.

For lipid-protein overlay assays, PIP strips containing 15 purified lipids (P-6001, Echelon Bioscience) were covered with 10 mL of PBS-T blocking buffer (140-mM NaCl, 2.7-mM KCl, and 10-mM Na_2HPO_4, 1.8-mM KH_2PO_4, and 0.1% [v/v] Tween 20; pH 7.3) + 3% (w/v) BSA-fatty acid free and gently agitated for 2 h at room temperature (RT). The strips were incubated with 1 µg·±mL^{-1} purified proteins in 10 mL of PBS-T with 3% (w/v) BSA-fatty acid free at RT for 2 h. The strips were subjected to five 10-min washes with PBS-T and incubated with 1:10,000 anti-GST primary antibody (Abmart, M20007) in 10 mL of 3% (w/v) BSA-fatty acid free in PBS-T at RT for 1 h. The strips were subjected to five 10-min washes with PBS-T and incubated with secondary anti-mouse IgG (whole-molecule)-peroxidase antibody (Sigma Aldrich, A9044) at 1:10,000 dilution in 10 mL of PBS-T with 3% (w/v) BSA-fatty acid free at RT for 1 h. The strips were subjected to five 10-min washes with PBS-T. Images were obtained at RT using chemiluminescent signals.

Immunoblot analysis

Immunoblot analysis was performed as described previously (Zhou et al., 2020). Briefly, immunoblot analysis was performed on polyvinylidene fluoride (PVDF) membranes (Hybond-P, GE) using an anti-glutathione S-transferase (GST) primary antibody (Abmart, M20007) and secondary anti-mouse IgG (whole-molecule)-peroxidase antibody (Sigma Aldrich, A9044). The blots were incubated at RT for 1 h. The signals were visualized using Amersham ECL Prime Western Blotting Detection Reagents (GE) and detected with Amersham Imager 600 (GE).

Statistical analysis

Statistical analyses were performed using the SPSS software package (version 22.0; IBM). As described in the corresponding figure legends, the data are presented as means ± SD/SE from at least three independent replicates of developing seed number, pollen tube ovule targeting efficiency, relative pollen tube length, and semi-in-vivo pollen tube growth/LURE1.2-responsive assay. Two-tailed Student's *t* tests (*t* tests) were performed to determine the statistical significance, and the threshold was set to 0.05.

Accession numbers

Sequence data from this article can be found in the GenBank/EMBL libraries under the following accession numbers: At-*ALA3* (AT1G59820), At-*ALA1* (AT5G04930), At-*ALA6* (AT1G54280), At-*ALA7* (AT3G13900), At-*ALA9* (AT1G68710), At-*ALA12* (AT1G26130), At-*RabA4d* (AT3G 12160), At-*PRK1* (AT5G35390), At-*PRK2*(AT2G07040), At-*PRK3* (AT3G42880), At-*PRK4* (AT3G20190), At-*PRK5* (AT1G 50610), At-*PRK6* (AT5G20690), At-*PRK7* (AT4G31250), At-*PRK8* (AT1G72460).

Supplemental data

The following materials are available in the online version of this article.

Supplemental Figure S1. Loss of ALA3 function results in male sterility.

Supplemental Figure S2. Subcellular localization of PRK2, PRK4, and PRK5 in *ala3* mutants.

Supplemental Figure S3. Some members of the PRK family bind to anionic phospholipids in vivo and in vitro.

Supplemental Figure S4. *ala* mutant pollen tubes are wavy in response to AtLURE1.2.

Supplemental Figure S5. Sequence alignment of the carboxy-terminal domains of PRKs.

Supplemental Table S1. Primers used in this study.

Supplemental Data Set S1. Amino acid sequences of the intracellular JM domain of LRR-RLKs.

Supplemental Movie S1. Tip localization of PRK6–mRuby2 in *prk6* mutant pollen tubes.

Supplemental Movie S2. Tip localization of PRK3–mClover in *prk3 prk6* mutant pollen tubes.

Supplemental Movie S3. PRK6–mRuby2 moves in a disordered manner at the apical membrane, the apical membrane-proximal region, and the subapical region of *ala3 prk6* mutant pollen tubes.

Supplemental Movie S4. PRK3–mClover moves in a disordered manner at the apical membrane, the apical membrane-proximal region, and the subapical region of *ala3 prk3 prk6* mutant pollen tubes.

Supplemental Movie S5. Tip localization of PRK6–mRuby2 in *prk6* mutant pollen tubes.

Supplemental Movie S6. PRK6–mRuby2 moves in a disordered manner at the inverted cone zone of *raba4d prk6* mutant pollen tubes.

Supplemental Movie S7. Tip localization of PRK6–GFP in *prk6* pollen tubes.

Supplemental Movie S8. PRK6^{6Q}–GFP signals extend to the shank plasma membrane and decrease at the apical region of *prk6* mutant pollen tubes.

Supplemental Movie S9. PRK6^{8Q}–GFP signals are significantly reduced at the apical plasma membrane and in the vesicle-rich inverted cone zone of *prk6* pollen tubes but are significantly increased in the shank plasma membrane.

Supplemental Movie S10. Tip localization of PRK3–GFP in *prk3 prk6* pollen tubes.

Supplemental Movie S11. PRK3^{8Q}–GFP signals are present in the organelles and are increased in the shank plasma membrane of *prk3 prk6* pollen tubes.

Supplemental Movie S12. PRK3^{9Q}–GFP signals are increased in the organelles and extend to the shank plasma membrane of *prk3 prk6* pollen tubes.

References

Andersen JP, Vestergaard AL, Mikkelsen SA, Mogensen LS, Chalat M, Molday RS (2016) P4-ATPases as phospholipid flippases-structure, function, and enigmas. Front Physiol **7**: 275

Barbosa IC, Schwechheimer C (2014) Dynamic control of auxin transport-dependent growth by AGCVIII protein kinases. Curr Opin Plant Biol **22**: 108–115

Beer KB, Rivas-Castillo J, Kuhn K, Fazeli G, Karmann B, Nance JF, Stigloher C, Wehman AM (2018) Extracellular vesicle budding is inhibited by redundant regulators of TAT-5 flippase localization and phospholipid asymmetry. Proc Natl Acad Sci USA **115**: e1127–e1136

Berger F, Hamamura Y, Ingouff M, Higashiyama T (2008) Double fertilization-caught in the act. Trends Plant Sci **13**: 437–443

Bigay J, Antonny B (2012) Curvature, lipid packing, and electrostatics of membrane organelles: defining cellular territories in determining specificity. Dev Cell **23**: 886–895

Chen C, Ingram MF, Rosal PH, Graham TR (1999) Role for Drs2p, a P-type ATPase and potential aminophospholipid translocase, in yeast late Golgi function. J Cell Biol **147**: 1223–1236

Cheung AY, Wu HM (2008) Structural and signaling networks for the polar cell growth machinery in pollen tubes. Annu Rev Plant Biol **59**: 547–572

Clough SJ, Bent AF (1998) Floral dip: a simplified method for Agrobacterium-mediated transformation of Arabidopsis thaliana. Plant J **16**: 735–743

Dalton LE, Bean BDM, Davey M, Conibear E (2017) Quantitative high-content imaging identifies novel regulators of Neo1 traffcking at endosomes. Mol Biol Cell **28**: 1539–1550

Di Paolo G, De Camilli P (2006) Phosphoinositides in cell regulation and membrane dynamics. Nature **443**: 651–657

Dubois GA, Jaillais Y (2021) Anionic phospholipid gradients: an uncharacterized frontier of the plant endomembrane network. Plant Physiol **185**: 577–592

Duckney P, Deeks MJ, Dixon MR, Kroon J, Hawkins TJ, Hussey PJ (2017) Actin–membrane interactions mediated by NETWORKED2 in *Arabidopsis* pollen tubes through associations with pollen receptor-like kinase 4 and 5. New Phytol **216**: 1170–1180

Endo S, Shinohara H, Matsubayashi Y, Fukuda H (2013) A novel pollen-pistil interaction conferring high-temperature tolerance during reproduction via CLE45 signaling. Curr Biol **23**: 1670–1676

Gomès E, Jakobsen MK, Axelsen KB, Geisler M, Palmgren MG (2000) Chilling tolerance in *Arabidopsis* involves ALA1, a member of a new family of putative aminophospholipid translocases. Plant Cell **12**: 2441–2454

Guo Y, Qin G, Gu H, Qu L-J (2009) Dof5.6/HCA2, a Dof transcription factor gene, regulates interfascicular cambium formation and vascular tissue development in Arabidopsis. Plant Cell **21**: 3518–3534

Guo J, Yang Z (2020) Measuring exocytosis rate in *Arabidopsis* pollen tubes using corrected fluorescence recovery after photoconversion (cFRAPc) technique. Methods Mol Biol **2160**: 293–306

Guo Z, Lu J, Wang X, Zhan B, Li W, Ding SW (2017) Lipid flippases promote antiviral silencing & the biogenesis of viral & host siRNAs in *Arabidopsis*. Proc Natl Acad Sci USA **114**: 1377–1382

Hempel F, Stenzel I, Heilmann M, Krishnamoorthy P, Menzel W, Golbik R, Helm S, Dobritzsch D, Baginsky S, Lee J, et al. (2017) MAPKS influence pollen tube growth by controlling the formation of phosphatidylinositol 4,5-bisphosphate in an apical plasma membrane domain. Plant Cell **29**: 3030–3050

Heo WD, Inoue T, Park WS, Kim ML, Park BO, Wandless TJ, Meyer T (2006) PI(3,4,5)P3 and PI(4,5)P2 lipids target proteins with polybasic clusters to the plasma membrane. Science **314**: 1458–1461

Hepler PK, Vidali L, Cheung AY (2001) Polarized cell growth in higher plants. Annu Rev Cell Dev Biol **17**: 159–187

Higashiyama T, Takeuchi H (2015) The mechanism and key molecules involved in pollen tube guidance. Annu Rev Plant Biol **66**: 393–413

Hou S, Shi J, Hao L, Wang Z, Liao Y, Gu H, Dong J, Dresselhaus T, Zhong S, Qu LJ (2021) VPS18-regulated vesicle trafficking controls the secretion of pectin and its modifying enzyme during pollen tube growth in *Arabidopsis*. Plant Cell **33**: 3042–3056

Hua Z, Fatheddin P, Graham TR (2002) An essential subfamily of Drs2p-related P-Type ATPases is required for protein trafficking between Golgi complex and endosomal/vacuolar system. Mol Biol Cell **13**: 4100–4109

Hua Z, Graham TR (2003) Requirement for neo1p in retrograde transport from the Golgi complex to the endoplasmic reticulum. Mol Biol Cell **14**: 4971–4983

Huang WJ, Liu HK, McCormick S, Tang WH (2014) Tomato pistil factor STIG1 promotes in vivo pollen tube growth by binding to phosphatidylinositol 3-phosphate and the extracellular domain of the pollen receptor kinase LePRK2. Plant Cell **26**: 2505–2523

Jaillais Y, Hothorn M, Belkhadir Y, Dabi T, Nimchuk ZL, Meyerowitz EM, Chory J (2011) Tyrosine phosphorylation controls brassinosteroid receptor activation by triggering membrane release of its kinase inhibitor. Genes Dev **25**: 232–237

Johnson MA, Harper JF, Palanivelu R (2019) A fruitful journey: pollen tube navigation from germination to fertilization. Annu Rev Plant Biol **70**: 809–837

Kost B, Lemichez E, Spielhofer P, Hong Y, Tolias K, Carpenter C, Chua N (1999) Rac homologues and compartmentalized phosphatidylinositol 4, 5-bisphosphate act in a common pathway to regulate polar pollen tube growth. J Cell Biol **145**: 317–330

Lausser A, Dresselhaus T (2010) Sporophytic control of pollen tube growth and guidance in grasses. Biochem Soc Trans **38**: 631–634

Lee S, Uchida Y, Wang J, Matsudaira T, Nakagawa T, Kishimoto T, Mukai K, Inaba T, Kobayashi T, Molday RS, et al. (2015) Transport through recycling endosomes requires EHD 1 recruitment by a phosphatidylserine translocase. EMBO J **34**: 669–688

Liu C, Shen L, Xiao Y, Vyshedsky D, Peng C, Sun X, Liu Z, Cheng L, Zhang H, Han Z, et al. (2021) Pollen PCP-B peptides unlock a stigma peptide-receptor kinase gating mechanism for pollination. Science **372**: 171–175

Liu K, Surendhran K, Nothwehr SF, Graham TR (2008) P4-ATPase requirement for AP-1/clathrin function in protein transport from the trans-golgi network and early endosomes. Mol Biol Cell **20**: 2673–2683

Liu J, Zhong S, Guo X, Hao L, Wei X, Huang Q, Hou Y, Shi J, Wang C, Gu H, Qu LJ (2013) Membrane-bound RLCKs LIP1 and LIP2 are essential male factors controlling male-female attraction in *Arabidopsis*. Curr Biol **23**: 993–998

López-Marqués RL (2021) Lipid flippases in polarized growth. Curr Genet **67**: 255–262

López-Marqués RL, Davis JA, Harper JF, Palmgren M (2021) Dynamic membranes: the multiple roles of P4 and P5 ATPases. Plant Physiol **185**: 619–631

Martzoukou O, Amillis S, Zervakou A, Christoforidis S, Diallinas G (2017) The AP-2 complex has a specialized clathrin-independent role in apical endocytosis and polar growth in fungi. eLife **6**: e20083

Márton ML, Cordts S, Broadhvest J, Dresselhaus T (2005) Micropylar pollen tube guidance by egg apparatus 1 of maize. Science **307**: 573–576

Meng JG, Zhang MX, Yang WC, Li HJ (2019) TICKET attracts pollen tubes and mediates reproductive isolation between relative species in Brassicaceae. Sci China Life Sci **62**: 1413–1419

McCormick S (2004) Control of male gametophyte development. Plant Cell **16**: 142–153

McDowell SC, López-Marqués RL, Poulsen LR, Palmgren MG, Harper JF (2013) Loss of the *Arabidopsis thaliana* P4-ATPase ALA3 reduces adaptability to temperature stresses and impairs vegetative, pollen, and ovule development. PLoS One **8**: 1–11

McGough IJ, de Groot REA, Jellett AP, Betist MC, Varandas KC, Danson CM, Heesom KJ, Korswagen HC, Cullen PJ (2018) SNX3-retromer requires an evolutionary conserved MON2:DOPEY2:ATP9A complex to mediate Wntless sorting and Wnt secretion. Nat Commun **9**: 3737

McDowell SC, López-Marqués RL, Poulsen LR, Palmgren MG, Harper JF (2018) Loss of the *Arabidopsis thaliana* P4-ATPase ALA3 reduces adaptability to temperature stresses and impairs vegetative, pollen, and ovule development. PLoS One **8**: e62577

McDowell SC, López-Marqués RL, Cohen T, Brown E, Rosenberg A, Palmgren MG, Harper JF (2015) Loss of the *Arabidopsis thaliana* P4-ATPases ALA6 and ALA7 impairs pollen fitness and alters the pollen tube plasma membrane. Front Plant Sci **6**: 197

Muschietti J, Dircks L, Vancanneyt G, McCormick S (1994) LAT52 protein is essential for tomato pollen development: pollen expressing antisense LAT52 RNA hydrates and germinates abnormally and cannot achieve fertilization. Plant J **6**: 321–338

Muthusamy BP, Natarajan P, Zhou X, Graham TR (2009) Linking phospholipid flippases to vesicle-mediated protein transport. Biochim Biophys Acta **1791**: 612–619

Niu Y, Qian D, Liu B, Ma J, Wan D, Wang X, He W, Xiang Y (2017) ALA6, a P4-type ATPase, is involved in heat stress responses in Arabidopsis thaliana. Front Plant Sci **8**: 1–13

Okuda S, Tsutsui H, Shiina K, Sprunck S, Takeuchi H, Yui R, Kasahara RD, Hamamura Y, Mizukami A, Susaki D, et al. (2009) Defensin-like polypeptide LUREs are pollen tube attractants secreted from synergid cells. Nature **458**: 357–361

Palmgren MG, Nissen P (2011) P-type ATPases. Annu Rev Biophys **40**: 243–266

Platre MP, Noack LC, Doumane M, Bayle V, Simon MLA, Maneta-Peyret L, Fouillen L, Stanislas T, Armengot L, Pejchar P et al. (2018) A Combinatorial Lipid Code Shapes the Electrostatic Landscape of Plant Endomembranes. Dev Cell **45**: 465–480.e11

Pomorski T, Lombardi R, Riezman H, Devaux PF, van Meer G, Holthuis JC (2003) Drs2p-related P-type ATPases Dnf1p and Dnf2p are required for phospholipid translocation across the yeast plasma membrane and serve a role in endocytosis. Mol Biol Cell **14**: 1240–1254

Potocký M, Pleskot R, Pejchar P, Vitale N, Kost B, Žárský V (2014) Live-cell imaging of phosphatidic acid dynamics in pollen tubes visualized by Spo20p-derived biosensor. New Phytol **203**: 483–494

Poulsen LR, López-Marqués RL, McDowell SC, Okkeri J, Licht D, Schulz A, Pomorski T, Harper JF, Palmgren MG (2008) The *Arabidopsis* P4-ATPase ALA3 localizes to the Golgi and requires a β-subunit to function in lipid translocation and secretory vesicle formation. Plant Cell **20**: 658–676

Poulsen LR, López-Marqués RL, Pedas PR, McDowell SC, Brown E, Kunze R, Harper JF, Pomorski TG, Palmgren M (2015) A phospholipid uptake system in the model plant *Arabidopsis thaliana*. Nat Commun **6**: 7649

Roland BP, Graham TR (2014) Decoding P4-ATPase substrate interactions. Crit Rev Biochem Mol Biol **51**: 513–527

Ruan H, Li J, Wang T, Ren H (2021) Secretory vesicles targeted to plasma membrane during pollen germination and tube growth. Front Cell Dev Biol 8: 615447

Schultzhaus Z, Yan H, Shaw BD (2015) *Aspergillus nidulans* flippase DnfA is cargo of the endocytic collar and plays complementary roles in growth and phosphatidylserine asymmetry with another flippase, DnfB. Mol Microbiol 97: 18–32

Shimizu KK, Okada K (2000) Attractive and repulsive interactions between female and male gametophytes in *Arabidopsis* pollen tube guidance. Development 127: 4511–4518

Simon ML, Platre MP, Marquès-Bueno MM, Armengot L, Stanislas T, Bayle V, Caillaud MC, Jaillais Y (2016) A PtdIns(4)P-driven electrostatic field controls cell membrane identity and signalling in plants. Nat Plants 2: 16089

Szumlanski AL, Nielsen E (2009) The rab GTPase RabA4d regulates pollen tube tip growth in *Arabidopsis thaliana*. Plant Cell 21: 526–544

Takeuchi H, Higashiyama T (2012) A species-specific cluster of defensin-like genes encodes diffusible pollen tube attractants in *Arabidopsis*. PLoS Biol 10: e1001449

Takeuchi H, Higashiyama T (2016) Tip-localized receptors control pollen tube growth and LURE sensing in *Arabidopsis*. Nature 531: 245–248

Takeuchi H (2021) The role of diverse LURE-type cysteine-rich peptides as signaling molecules in plant reproduction. Peptides 142: 170572

Tang W, Ezcurra I, Muschietti J, McCormick S (2002) A cysteine-rich extracellular protein, LAT52, interacts with the extracellular domain of the pollen receptor kinase LePRK2. Plant Cell 14: 2277–2287

Tang W, Kelley D, Ezcurra I, Cotter R, McCormick S (2004) LeSTIG1, an extracellular binding partner for the pollen receptor kinases LePRK1 and LePRK2, promotes pollen tube growth in vitro. Plant J 39: 343–353

Underwood CJ, Henderson IR, Martienssen RA (2017) Genetic and epigenetic variation of transposable elements in *Arabidopsis*. Curr Opin Plant Biol 36: 135–141

Vermeer JEM, Van Leeuwen W, Tobeña-Santamaria R, Laxalt AM, Jones DR, Divecha N, Gadella TWJ, Munnik T (2006) Visualization of PtdIns3P dynamics in living plant cells. Plant J 47: 687–700

Wang F, Li X, Li Y, Han J, Chen Y, Zeng J, Su M, Zhuo J, Ren H, Liu H, et al. (2021) *Arabidopsis* P4 ATPase-mediated cell detoxification confers resistance to Fusarium graminearum and Verticillium dahliae. Nat Commun 12: 6426

Wang T, Liang L, Xue Y, Jia PF, Chen W, Zhang MX, Wang YC, Li HJ, Yang WC (2016) A receptor heteromer mediates the male perception of female attractants in plants. Nature 531: 241–244

Wang X, Sheng X, Tian X, Zhang Y, Li Y (2020) Organelle movement and apical accumulation of secretory vesicles in pollen tubes of *Arabidopsis thaliana* depend on class XI myosins. Plant J 104: 1685–1697

Wehman AN, Poggioli C, Schweinsberg P, Grant BD, Nance J (2011) The P4-ATPase TAT-5 inhibits the budding of extracellular vesicles in C. elegans embryos. Science 7: 221–229

Wrzaczek M, Brosché M, Kollist H, Kangasjärvi J (2009) *Arabidopsis* GRI is involved in the regulation of cell death induced by extracellular ROS. Proc Natl Acad Sci USA 106: 5412–5417

Wrzaczek M, Vainonen JP, Stael S, Tsiatsiani L, Help-Rinta-Rahko H, Gauthier A, Kaufholdt D, Bollhöner B, Lamminmäki A, Staes A, et al. (2015) GRIM REAPER peptide binds to receptor kinase PRK 5 to trigger cell death in *Arabidopsis*. EMBO J 34: 55–66

Wu Y, Takar M, Cuentas-Condori AA, Graham TR (2016) Neo1 and phosphatidylethanolamine contribute to vacuole

membrane fusion in saccharomyces cerevisiae. Cell Logist 6: e1228791

Xiang Y, Huang X, Wang T, Zhang Y, Liu Q, Hussey PJ, Ren H (2007) ACTIN BINDING PROTEIN 29 from Lilium pollen plays an important role in dynamic actin remodeling. Plant Cell 19: 1930–1946

Xu P, Baldridge RD, Chi RJ, Burd CG, Graham TR (2013) Phosphatidylserine flipping enhances membrane curvature and negative charge required for vesicular transport. J Cell Biol 202: 875–886

Xu P, Hankins HM, MacDonald C, Erlinger SJ, Frazier MN, Diab NS, Piper RC, Jackson LP, MacGurn JA, Graham TR (2017) COPI mediates recycling of an exocytic SNARE by recognition of a ubiquitin sorting signal. eLife 6: e28342

Yang K, Wang L, Le J, Dong J (2020) Cell polarity: regulators and mechanisms in plants. J Integr Plant Biol 62: 132–147

Yeung T, Gilbert GE, Shi J, Silvius J, Kapus A, Grinstein S (2008) Membrane phosphatidylserine regulates surface charge and protein localization. Science 319: 210–213

Yu X, Zhang X, Zhao P, Peng X, Chen H, Bleckmann A, Bazhenova A, Shi C, Dresselhaus T, Sun MX (2021) Fertilized egg cells secrete endopeptidases to avoid polytubey. Nature 592: 433–437

Yu Y, Song J, Tian X, Zhang H, Li L, Zhu H (2018) *Arabidopsis* PRK6 interacts specifically with AtRopGEF8/12 and induces depolarized growth of pollen tubes when overexpressed. Sci China Life Sci 61: 100–112

Zhang D, Wengier D, Shuai B, Gui CP, Muschietti J, McCormick S, Tang WH (2008) The pollen receptor kinase LePRK2 mediates growth-promoting signals and positively regulates pollen germination and tube growth. Plant Physiol 148: 1368–1379

Zhang J, Yue L, Wu X, Liu H, Wang W (2021) Function of small peptides during male-female crosstalk in plants. Front Plant Sci 12: 671196

Zhang X, Adamowski M, Marhava P, Tan S, Zhang Y, Rodriguez L, Zwiewka M, Pukyšová V, Sánchez AS, Raxwal VK, et al. (2020) *Arabidopsis* flippases cooperate with ARF GTPase exchange factors to regulate the trafficking and polarity of PIN auxin transporters. Plant Cell 32: 1644–1664

Zhang X, Liu W, Nagae TT, Takeuchi H, Zhang H, Han Z, Higashiyama T, Chai J (2017) Structural basis for receptor recognition of pollen tube attraction peptides. Nat Commun 8: 1331

Zhang X, Oppenheimer DG (2009) IRREGULAR TRICHOME BRANCH 2 (ITB2) encodes a putative aminophospholipid translocase that regulates trichome branch elongation in *Arabidopsis*. Plant J 60: 195–206

Zhao XY, Wang Q, Li S, Ge FR, Zhou LZ, McCormick S, Zhang Y (2013) The juxtamembrane and carboxy-terminal domains of *Arabidopsis* PRK2 are critical for ROP-induced growth in pollen tubes. J Exp Bot 64: 5599–5610

Zhao Y, Yan A, Feijó JA, Furutani M, Takenawa T, Hwang I, Fu Y, Yang Z (2010) Phosphoinositides regulate clathrin-dependent endocytosis at the tip of pollen tubes in *Arabidopsis* and *tobacco*. Plant Cell 22: 4031–4044

Zhong S, Liu M, Wang Z, Huang Q, Hou S, Xu YC, Ge Z, Song Z, Huang J, Qiu X, et al. (2019) Cysteine-rich peptides promote interspecific genetic isolation in *Arabidopsis*. Science 364: e9564

Zhong S, Qu LJ (2019) Peptide/receptor-like kinase-mediated signaling involved in male-female interactions. Curr Opin Plant Biol 51: 7–14

Zhou Y, Yang Y, Niu Y, Fan TT, Qian D, Luo C, Shi Y, Li S, An L, Xiang Y (2020) The tip-localized phosphatidylserine established by *Arabidopsis* ALA3 is crucial for rab GTPase-mediated vesicle trafficking and pollen tube growth. Plant Cell 32: 3170–3187